JGR Oceans

RESEARCH ARTICLE
10.1029/2024JC021079

What Drives the Mean Along-Shelf Flow in the Northwest Atlantic Coastal Ocean?

Ke Chen[1] and **Jiayan Yang**[1]

[1]Department of Physical Oceanography, Woods Hole Oceanographic Institution, Woods Hole, MA, USA

Key Points:

- Wind forcing plays an important role in setting up the mean along-shelf flow in the Northwest Atlantic (NWA) coastal ocean
- Local buoyancy from continental runoff is not as significant as previously hypothesized
- Remote subpolar inflow is an essential part of the NWA shelf circulation system

Correspondence to:

K. Chen,
kchen@whoi.edu

Citation:

Chen, K., & Yang, J. (2024). What drives the mean along-shelf flow in the Northwest Atlantic coastal ocean? *Journal of Geophysical Research: Oceans*, *129*, e2024JC021079. https://doi.org/10.1029/2024JC021079

Received 8 APR 2024
Accepted 5 JUL 2024

Author Contributions:

Conceptualization: Ke Chen, Jiayan Yang
Data curation: Ke Chen
Formal analysis: Ke Chen
Funding acquisition: Ke Chen, Jiayan Yang
Investigation: Ke Chen, Jiayan Yang
Methodology: Ke Chen, Jiayan Yang
Project administration: Ke Chen, Jiayan Yang
Resources: Ke Chen
Software: Ke Chen
Validation: Ke Chen
Visualization: Ke Chen
Writing – original draft: Ke Chen
Writing – review & editing: Ke Chen, Jiayan Yang

Abstract A long-standing hypothesis is that the steady along-shelf circulation in the Northwest Atlantic (NWA) coastal ocean is driven by buoyancy input from continental freshwater runoff. However, the forcing from the freshwater runoff has not been adequately evaluated and compared with other potential driving mechanisms. This study investigates the roles of both wind stress and freshwater runoff in driving the mean along-shelf flow in the NWA coastal ocean and examines other potential drivers using a newly developed high-resolution regional model with realistic forcing conditions. The results reveal that wind stress has a larger impact than freshwater runoff on the overall mean circulation and along-shelf sea-level gradient on the NWA shelf. While the continental freshwater input consistently contributes to the equatorward along-shelf flow and higher sea level along the coast, wind stress is more effective for the setup of the broad-scale circulation pattern by driving the along-shelf flow on the Labrador Shelf and opposing the flow in the Mid-Atlantic Bight and on the Scotian Shelf. In addition to the local wind and continental runoff, the sub-Arctic inflow from higher latitude is an essential part of the NWA shelf circulation system. This remote driver directly contributes to the along-shelf flow and insulates the shelf flow from the Gulf Stream on the southern shelves.

Plain Language Summary This study addresses a long-standing question of what drives the mean equatorward flow along the Northwest Atlantic continental shelf. The results show that the mean along-shelf flow is influenced more by wind stress than local buoyancy forcing resulting from the freshwater discharges from rivers and glaciers, which has long been considered the dominant driver of the along-shelf circulation. Remote forcing through inflow from higher latitude is also important in maintaining the broad-scale mean along-shelf flow and sea level. This work also provides updated views of the circulation dynamics and momentum balance of the mean along-shelf circulation, contributing to the understanding of both the current and future states of our ocean and climate systems.

1. Introduction

The Northwest Atlantic (NWA) continental shelf extending from Cape Chidley to Cape Hatteras lies in the western boundary confluence zone of the North Atlantic Subpolar Gyre and North Atlantic Subtropical Gyre (Figure 1). The shelf and shelfbreak circulation in the NWA are dominated by equatorward along-isobath flows, which originate at higher latitude (e.g., Chapman & Beardsley, 1989; Fratantoni & Pickart, 2007; Loder et al., 1998; Smith & Schwing, 1991). The regional circulation dynamics are influenced by both the multi-branch Labrador current (Lazier & Wright, 1993) to the north and the Gulf Stream to the south, along with other influences from wind, buoyancy, inflow from the Arctic, and other processes such as tides and bathymetry (Loder et al., 1998). These factors make the NWA shelf one of the most dynamically complex regions in the world oceans.

It has long been hypothesized that the steady circulation system over the entire NWA shelf is primarily buoyancy-driven by freshwater fluxes from river runoff and glacier melt starting from the southern Greenland coast (Chapman & Beardsley, 1989). Over the Labrador Shelf, observations from CTDs (Conductivity-Temperature-Depth) and current meters confirm the dominance of buoyancy flux in driving the annual cycle of the Labrador Shelf Current (Lazier & Wright, 1993), despite annual-mean wind stress being in the same direction as the mean along-shelf flow. Instead, wind is only considered important in driving the Labrador Slope current through Sverdrup return flow (Lazier & Wright, 1993; Loder et al., 1998; Thompson et al., 1986). In the southern part of this shelf flow system, because the mean wind stress is against the mean along-shelf flow (Figure 1), the along-shelf pressure gradient (along-shelf sea level tilt, to be exact) has been considered as an important driver of the along-shelf flow as it is required to balance the surface wind stress and bottom stress (Lentz, 2008; Scott &

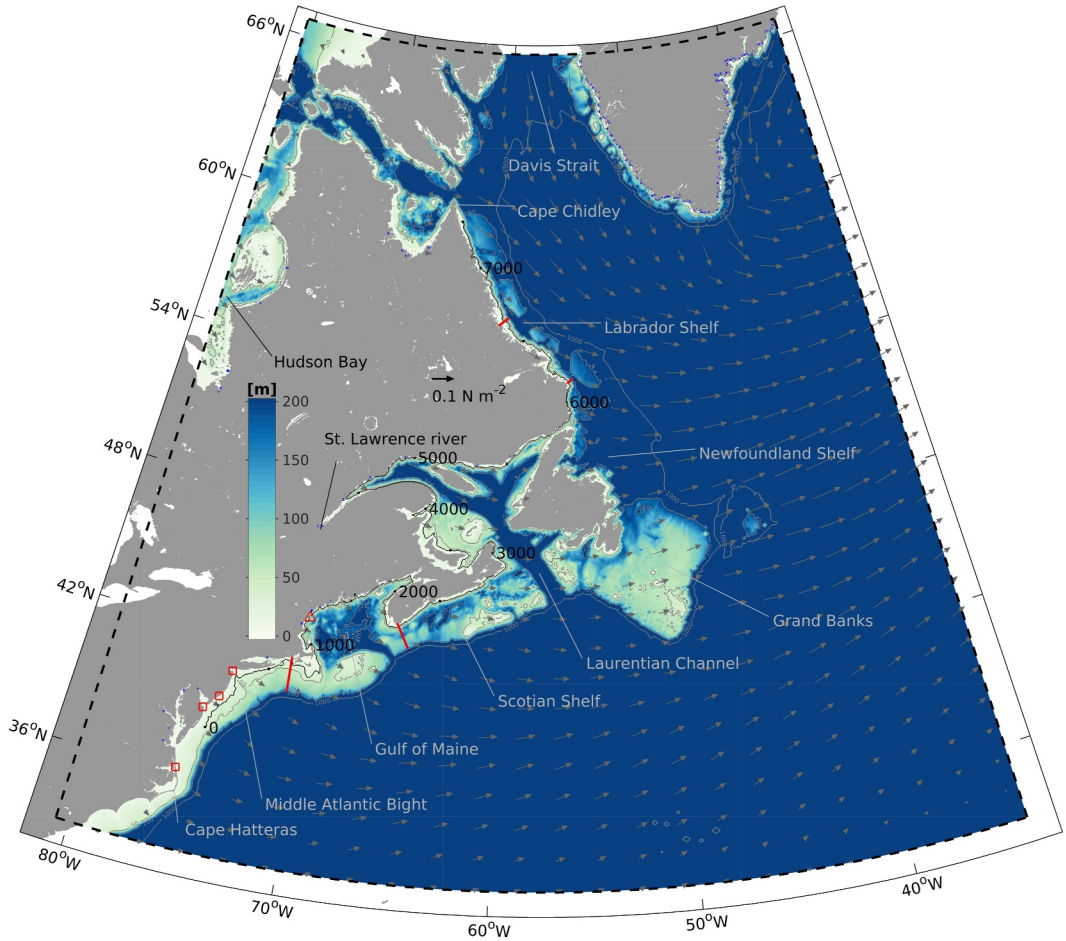

Figure 1. Map showing the Northwest Atlantic (NWA). The model domain is bounded by the dashed black lines. Water depth in the model is shown in color with the color range (200 m) chosen to illustrate the continental shelf topography. 50, 200, and 1,000 m isobaths are contoured in gray. The 30 m isobath is contoured in black with distance (in km) labeled. Four cross-shelf sections extending from the coast to the 200 m isobath are shown in red. Freshwater point sources implemented in the model are shown as blue dots. Locations of four tidal gauges in the Mid-Atlantic Bight are shown as squares. Location of NERACOOS/GoMOOS mooring B (Section 2.2.2) is shown as a triangle. Dark gray vectors are the climatological mean wind stress. Major geographic regions are labeled.

Csanady, 1976; Stommel & Leetmaa, 1972). This along-shelf pressure gradient could be related to remote buoyancy anomaly (Pringle, 2018), or imposed by offshore larger-scale circulation (Beardsley & Winant, 1979; Csanady, 1978). Previous works using simple barotropic models suggest that offshore pressure gradient associated with larger-scale circulation cannot penetrate on the shelf (Chapman et al., 1986; Wang, 1982). More recent studies, however, show that the large-scale deep ocean pressure gradient can penetrate onto the shelf in an attenuated and equatorward shifted form, indicating a potential role of remote forcing from the open ocean (Wise et al., 2018, 2020). The exact origin of the pressure gradient term in the entire NWA shelf system is not entirely clear.

While the importance of buoyancy forcing for the NWA shelf circulation has been recognized, other potential drivers of the mean along-shelf flow have not been adequately investigated and the relative contributions have not been quantitatively addressed. A recent study aiming to examine the role of wind forcing in driving the large-scale shelf circulation in the NWA shows that wind stress alone is able to set up a shelf circulation pattern that is largely consistent with known features, despite the simple dynamics of the two-layer model that is used (Yang & Chen, 2021, YC21 hereafter). The annual mean along-shelf sea level gradient over the NWA shelf from the wind-driven two-layer model is about 3×10^{-8} to 4×10^{-8}, remarkably similar to an observation-based inference of 3.7×10^{-8} (Lentz, 2008) assuming simple dynamical balance. The annual cycle of the circulation and sea level

produced in the wind-driven model (YC21) is also largely consistent with prior observations and modeling results (Han et al., 2008; Hannah et al., 2001; Lazier & Wright, 1993; Wang et al., 2015; Wu et al., 2012). These results suggest that wind stress is likely an important driver of the NWA mean shelf circulation and should not be overlooked. The significance of wind-forcing warrants further investigation, particularly its comparison with buoyancy forcing from continental runoff (Chapman & Beardsley, 1989) as well as other processes beyond the regional setting such as larger-scale circulation.

The objective of this work is to comprehensively examine the driving processes of the mean along-shelf circulation in the NWA using a 3-D, primitive-equation, regional circulation model. This is one step beyond the two-layer wind-driven model used in YC21, which resolves only the barotropic component of the shelf circulation and does not include baroclinic factors such as the shelfbreak frontal system and freshwater fluxes. In comparison, the 3D model allows wind stress, continental freshwater discharge, as well as both regional and large-scale processes to be integrated and compared in a dynamically consistent setting. The overall goals are to improve the dynamical understanding of the drivers of the costal circulation system in the NWA and to provide an updated large-scale view of how the shelf circulation and variability are connected to broader scale processes.

The remainder of the paper is structured as follows. Section 2 describes the configuration of the primitive-equation regional circulation model, along with model skill assessment, and the designs of numerical experiments for comparing various forcing processes. In Section 3, we investigate the roles of wind stress and continental freshwater runoff in setting up the mean along-shelf flow. Simplified circulation dynamics along with a diagnosis of momentum balance are used to understand the responses of the along-shelf flow to wind stress and freshwater runoff. In Section 4, we describe the partition of the transport quantification and discuss the sub-Arctic inflow from higher latitude as a remote driver of the NWA shelf system. The role of sea ice on the northern shelves as well as remote wind- and buoyancy-driven contributions are also discussed, followed by summary and conclusions in Section 5.

2. Numerical Modeling

2.1. New Regional Model Development and Setup

A new high-resolution numerical model covering the entire NWA (i.e., NWA model, Figure 1) has been constructed based on the hydrostatic Regional Ocean Modeling System (ROMS). The ROMS is a free-surface, primitive equation model in widespread use for estuarine, coastal, and basin-scale ocean applications (www.myroms.org/papers). ROMS employs split-explicit separation of fast barotropic and slow baroclinic modes, and is formulated in vertically stretched terrain following coordinates using algorithms described in details by Shchepetkin and McWilliams (2005) and Haidvogel et al. (2008). A redefinition of the barotropic pressure-gradient term (Shchepetkin & McWilliams, 2005) is also applied in ROMS to reduce the pressure gradient truncation error. More details of ROMS can be found in the above two reviews.

The construction of this new high-resolution model is based on prior experience in developing and using several regional circulation models including the Shelfbreak model (Chen & He, 2010), MABGOM model (Chen & He, 2015; Chen et al., 2015, 2016), MABGOM2 model (Rypina et al., 2019), and NESS model (Chen et al., 2022) which all have been successfully used to investigate dynamics of shelf and slope processes in the region. For completeness, the setup of this new NWA model is briefly described below.

The horizontal resolution of the new NWA model ranges from 3 km in the lower latitude (32°N) to 1.5-km in the higher latitude (67°N), with an average resolution of 2 km. Vertically, there are 40 terrain-following layers with a carefully chosen stretching scheme to resolve both surface and bottom layers (minimum resolution 0.2 m over the shelf) and the water column. Smoothing of model bathymetry was done at a limited level to guarantee numerical stability. Sensitivity experiments were carried out for choosing relevant numerical parameters (e.g., baroclinic and barotropic time steps, background diffusivity) for the application. A generic-length scale (GLS) turbulent mixing closure k-kl scheme (Warner et al., 2005) was used to calculate vertical mixing. Bottom stress was calculated using a quadratic method with a drag coefficient of 0.003.

The configuration of the initial and open boundary conditions as well as surface forcings follows the same strategy of prior modeling work (e.g., Chen & He, 2015; Chen et al., 2015, 2022). The model's initial and boundary conditions are extracted from a combination of the mesoscale variability from a data assimilative global ocean reanalysis product, CMEMS GLORYS12v1 (Copernicus Marine Environment Monitoring Service GLobal

Ocean ReanalYsis and Simulation) (Lellouche et al., 2021), and the background mean fields from the temperature and salinity climatology of the 1/4° World Ocean Atlas (WOA) climatology (Garcia et al., 2019). The rationale is to remove the mean temperature and salinity biases in the global product, which is not optimized for shelf- and/or slope-scale dynamics due to the under-represented coastal processes including river freshwater flux and tides. In the correction, the climatological monthly means of temperature and salinity from the GLORYS data set were replaced by climatological monthly means from the WOA climatology while the variability, that is, the deviations from the climatological mean, was retained. Corresponding to the bias-correction of the temperature and salinity fields, the monthly mean depth-averaged geostrophic component of the velocity field separately calculated from WOA and GLORYS is also corrected in the same fashion for the boundary conditions.

Subtidal free surface and 2D momentum boundary conditions of the NWA model were derived from the corrected GLORYS fields using an explicit Chapman (1985) and Shchepetkin scheme (Mason et al., 2010), plus M2 tidal harmonics from the TPXO9 version 4 global tidal model (Egbert & Erofeeva, 2002). An Orlanski-type radiation boundary condition (Orlanski, 1976) was used for 3D state variables. A ∼200-km wide sponge/nudging zone is implemented along the south and east open boundaries for a smooth transition from the global model to the NWA model. The nudging strength decreases from the open boundary with a timescale of 2 days to a nudging-free interior. Laplacian horizontal diffusivity and viscosity are also linearly increased from the interior values 4 and 10 $m^2\ s^{-1}$ to tenfold along the open boundaries to effectively eliminate the wave reflections due to imperfect boundary conditions.

The surface forcing of the model combines air-sea fluxes calculated using bulk formulas and a surface thermal correction based on high-resolution SST maps. This scheme has been applied previously to provide realistic forcing of air-sea exchange (e.g., Chen et al., 2015; Chen et al., 2022; Chen & He, 2010). The bulk formulas calculation (Fairall et al., 2003) is based on three hourly and 0.125° resolution meteorological data (surface winds, air temperature, air pressure, relative humidity, short wave radiation, long wave radiation, cloud coverage, and precipitation) from the European Centre for Medium-Range Weather Forecasts (ECMWF) ERA5 global reanalysis (Hersbach et al., 2020). This calculation provides large-scale variability in the fluxes of momentum and buoyancy at the ocean surface, but it may contain uncertainties in reproducing some fine scale structures. To compensate for this deficiency in the surface forcing, the surface thermal correction adjusts the surface heat flux based on the difference of the model SST and the 1 km resolution Multi-scale Ultra-high Resolution (MUR) SST (Chin et al., 2017). The adjustment time scale is 3 hours (Chen et al., 2015), consistent with the temporal resolution of the ERA5 product.

Freshwater discharge from major rivers and glaciers in the model domain is implemented. Monthly runoff from 44 major rivers in North America is retrieved from a global river flow and continental discharge data set, which is based on streamflow measurements from stations and also considers the drainage effect to estimate the river-mouth outflow (Dai, 2021). Among these rivers, St. Lawrence River has the largest discharge rate, at $1.2 \times 10^4\ m^3 s^{-1}$ on average (Figure 2). A total of 16 rivers discharge into the Hudson Bay, with 5 rivers located within the model domain (Figure 1). To fully account for the freshwater discharge into the semi-closed Hudson Bay, the freshwater input from all 16 rivers is considered and distributed among the 5 rivers in the southeast of the Bay (within the model domain). Collectively, the total freshwater discharge into the Hudson Bay is $1.4 \times 10^4\ m^3 s^{-1}$, comparable to the discharge from the St. Lawrence River (Figure 2). Glacier discharge from Greenland is retrieved from JRA55-do, which is based on climatological (1958–2010) values of an existing data set (Bamber et al., 2012). A total of 150 point sources are implemented around southern Greenland (Figure 1). Cumulatively, they contribute a non-negligible portion of freshwater input of $5.6 \times 10^3\ m^3 s^{-1}$ into the NWA.

2.2. Realistic Modeling and Skill Assessment

The major utility of the new NWA model is to extend the results from the wind-driven model used in YC21 to a more realistic setting. As such, the model-data comparison below is a demonstration of the model's utility for process understanding instead of a full model validation. For the purpose of skill assessment, the new NWA model is first configured in realistic mode. Realistic initial and boundary conditions, surface forcing, and freshwater inputs are used to produce a hindcast simulation from 2003 to 2009. In the following, the model is compared against both broad-scale observation-derived products and in situ observations in the southern part of the NWA shelf system in the Middle Atlantic Bight (MAB) and Gulf of Maine (GoM), where more observations are available.

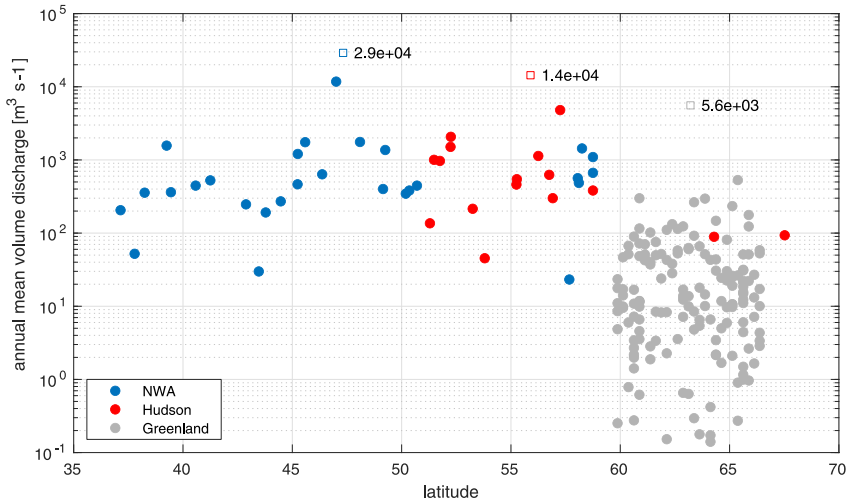

Figure 2. Climatological mean volume discharge rates from rivers and glaciers in the Northwest Atlantic. Three groups of freshwater point sources are color coded: rivers along most of the NWA coastline from Cape Hatteras to Labrador shelf are denoted in blue (largest discharge being from St. Lawrence River, $\sim 1.2 \times 10^4$ $m^3 s^{-1}$), rivers into the Hudson Bay are denoted in red, and glacier discharge points along southern Greenland are denoted in gray. Open squares represent the total volume discharge of freshwater from the three groups.

2.2.1. Broad Scale Climatological Hydrography and Surface Geostrophic Flow

The modeled annual mean surface temperature and salinity compare well with those from the National Centers for Environmental Information (NCEI) NWA Regional Climatology (Figure 3). The large-scale patterns of temperature and salinity are simulated reasonably well including along-shelf temperature gradient from north to south, contrast of temperature on the shelves and in the open ocean, and low salinity water in the Hudson Bay, near the St. Lawrence estuarine, and along the Mid-Atlantic Bight coast. Similarly, the model captures the large-scale geostrophic currents well (Figure 3). In comparison to the surface geostrophic velocity derived from the Copernicus Marine Environment Monitoring Service (CMEMS) Absolute Dynamic Topography (ADT), the Gulf Stream's main axis, its meanders to the east of the Grand Banks, and cyclonic circulation in the subpolar region are well represented. The high-resolution model also captures additional features missing from the CMEMS product including Labrador coastal current and shelfbreak jet off the continental shelf of the US northeast. The existence of these currents has been verified in previous studies (e.g., Lazier & Wright, 1993; Loder et al., 1998). In particular, the existence of the shelfbreak jet in the Mid-Atlantic Bight is reflected in the increasing depth-averaged flow from the inner shelf to the outer shelf (Lentz, 2008 and Figure 6 in Section 2.2.4). The geostrophic currents derived from the coarser resolution CMEMS ADT do not sufficiently represent these important features.

Possible causes for the differences between the observation-derived products and the NWA model include different resolutions (~10 km NCEI climatology, ~25 km CEMES ADT, and ~ 2 km NWA model), uncertainties of interpolations in the observational products, and imperfect model configurations and representations of processes (e.g., uncertainties in the initial and boundary conditions, atmospheric forcing conditions, and lack of a sea ice module). Nevertheless, the NWA model represents reasonably well both broad-scale and local scale features, particularly as a non-data-assimilative general circulation model.

2.2.2. Coastal Hydrography

The NWA model's skill in simulating the hydrographic conditions in the coastal ocean is evaluated using long-term mooring observations in the GoM. Northeastern Regional Association of Coastal Ocean Observing System (NERACOOS) maintains a set of moorings (formally known as GoMOOS moorings, operated by the Physical Oceanography Group at the University of Maine) in the GoM. Since 2001, these moorings have been providing valuable information about the environmental conditions in the GoM. Model solutions are compared against observed temperature and salinity recorded at multiple buoys, including mooring B (local water depth 62 m) in the western GoM (Figure 1). The NWA model captures the variability of temperature at 1, 20, and 50 m well,

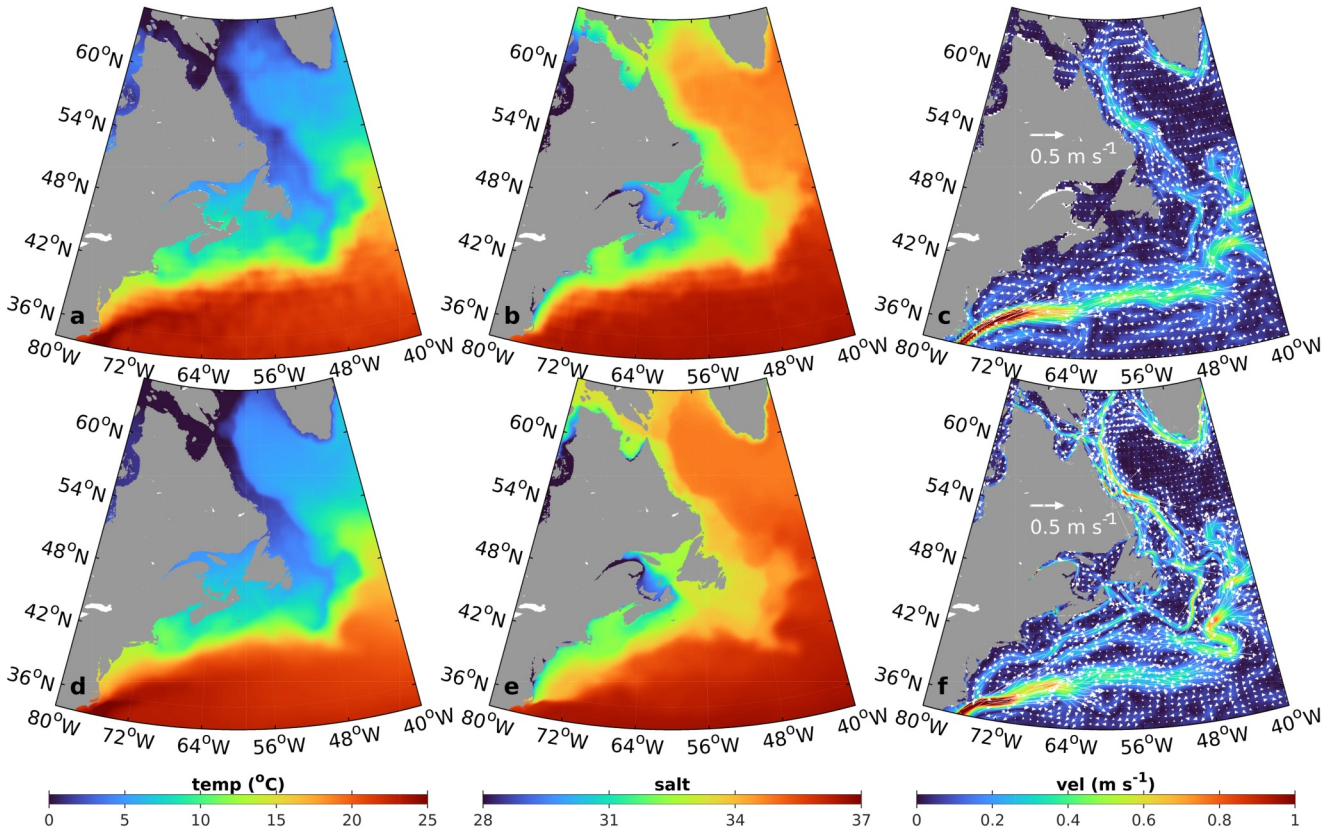

Figure 3. Comparison of climatological mean surface temperature (a, d), surface salinity (b, e), and surface geostrophic velocity (c, f) between observation-derived products (top panels: a, b, c) and the NWA model (lower panels: d, e, f). The surface temperature and salinity in a and b come from NOAA NCEI climatology (2005–2017 decadal mean). Surface geostrophic velocity in c is calculated from the gradient of long-term mean absolute dynamic topography from CMEMS gridded ADT during 2003–2009. The model fields are based on hindcast simulation of 2003–2009.

all with significant Pearson correlation coefficients larger than 0.85 and small mean bias (Figure 4). Temperature variability at depth is usually challenging to model as it requires a good representation of both advective fluxes (horizontal and vertical) and vertical mixing. The fact that the model generally tracks the temperature variability at 50 m indicates that these processes are properly represented by the model. Similar model/data agreements are found at other locations such as mooring A (water depth 65 m) and E (water depth 100 m) in the eastern GoM (not shown). In comparison to temperature, salinity variability is generally more challenging to model as it is sensitive to implementation of freshwater sources and proper representations of multi-scale buoyancy-driven processes, which involve advection, straining and mixing, and forcing factors such as wind and tides. Nevertheless, the NWA model reproduces the salinity in the coastal GoM remarkably well (Figure 4). Variability of salinity at surface (1 m), subsurface (20 m), and bottom (50 m) from sub-seasonal to interannual is well captured by the model. The correlation coefficients are all larger than 0.7, significant above the 99% confidence level using the effective degree of freedom (Emery & Thomson, 2001). The mean biases at the three depths are also very small (Figure 4). The consistency between the observations and the model demonstrates the skill of the NWA model in resolving dynamical processes determining the salinity field in a complex coastal region and the appropriate implementation of the freshwater point sources, which is an essential component of the buoyancy-driven system.

2.2.3. Coastal Sea Level

Point-by-point sea-level comparisons are made at four coastal tide gauges along the MAB coast (Figure 5). The seasonal cycle is removed from both modeled and observed sea level time series, which are then low-pass filtered with a 3-day cutoff window as the main interest here is sub-tidal signals. Direct comparisons show that the model can resolve sea level variations reasonably well in the simulation period. The majority of the sea level fluctuations

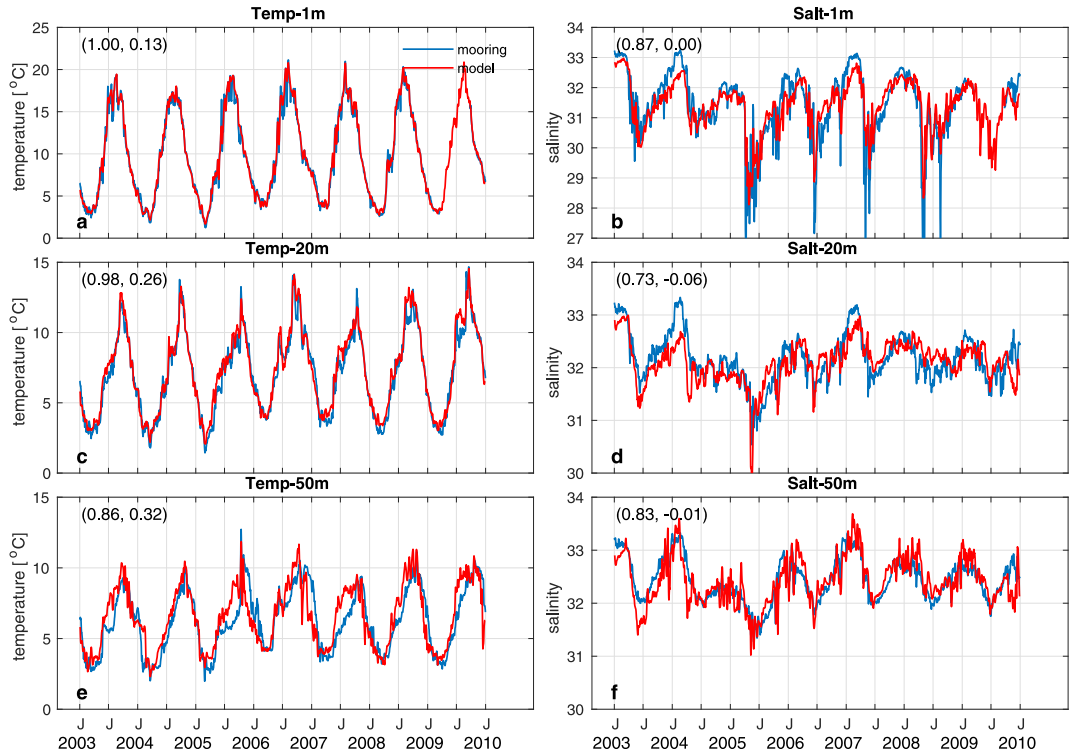

Figure 4. Comparison of temperature and salinity at surface (1 m), subsurface (20 m), and bottom (50 m) at NERACOOS/GoMOOS mooring B (see Figure 1 for the location) from 2003 to 2009. Observations are shown in blue and model data are shown in red. The linear correlation coefficients along with mean bias (model minus observation) are shown in each panel.

are consistent between the tide gauges and the model. The correlation coefficients between the two range from 0.68 to 0.82 at different stations, all significant above the 99% confidence level. Both wind-driven Ekman dynamics and continental shelf wave dynamics (e.g., Brink, 1991) dominate coastal sea level variations. The model-data agreements in coastal sea levels suggest that the model faithfully captures these dynamics in such a complex setting.

2.2.4. Mean Shelf Flow

As the primary focus here is the along-shelf flow, it is crucial that the model produces a credible shelf circulation. Long-term (>200 days) mean depth-averaged velocities from historical mooring sites across the MAB (Lentz, 2008) show that the mean flow is predominantly equatorward and approximately along-isobath. For a direct comparison, de-tided depth-averaged mean currents in the period of 2003–2009 from the NWA model are sampled at the same mooring locations (Figure 6). The comparison shows that the model successfully captures the predominantly equatorward flow. The magnitudes of velocities are largely consistent between the observation and model, with a linear correlation at 0.9. The overall direction of the modeled currents also compares well with the long-term observations, with less than 5° difference anti-clockwise. In particular, it is worth noting the excellent comparison at the southern New England shelf. The NWA model reproduces remarkably well the depth-averaged along-shelf currents that increase gradually with depth. The increasing along-shelf flow toward the deeper water is primarily a result of larger body force from the along-shelf pressure gradient term assuming constant pressure gradient on the shelf (Csanady, 1976). As a result, in the deep water a larger bottom stress is needed to balance the pressure gradient body force, leading to a larger bottom flow and thus depth-averaged flow (Lentz, 2008). The NWA model reproduces the cross-isobath pattern in depth-averaged along-shelf flow, indicating that relevant dynamical processes are appropriately represented.

2.3. Climatological Run and Sensitivity Experiments

Built upon the realistic configuration, the climatological state of the NWA shelf system is modeled to understand the dynamics of the mean shelf circulation. The initial and boundary conditions, surface forcings, and freshwater

Figure 5. Comparison of daily coastal sea level anomalies (seasonal cycle removed) along the Mid-Atlantic coast between the tidal gauges (blue) and model (red). Linear correlation coefficients are shown in each panel.

discharge rates are averaged over 2003–2017. To facilitate sensitivity experiments, wind stress, net heat flux, and net freshwater flux are directly imposed instead of using bulk flux calculations as in the realistic configuration. Everything else remains the same as the realistic configuration described in Section 2.1. To isolate the contribution from wind stress and freshwater runoff, sensitivity experiments without wind stress and freshwater sources within the model domain are conducted (designated as *noWind* and *noRiv* respectively), in addition to the control (*ctrl*) simulation. For each climatological run, the model is integrated forward until the system fully reaches a steady state, which is verified by the evolution of the total kinetic energy field within the model domain (not shown). The experiments take approximately 4–12 years to reach their respective steady states, with *ctrl* and *noRiv* experiments on the faster end and *noWind* and *closed* (Section 4) experiments taking longer. Only the solution from the last year of each model run is used for the analyses. In addition, an experiment with a closed northern boundary, that is, "*closed*" is conducted to evaluate the contribution of sub-Arctic inflow. In this experiment, the Davis Strait is closed and the ocean grids to the east of Greenland are masked out so that the sources of high-latitude inflow—the East Greenland Current and Baffin Current—are essentially shut down. Meanwhile, the southern and eastern open boundary conditions remain unchanged so that the Gulf Stream still enters the model domain, interacts with the internal processes, and exits the eastern boundary as the North Atlantic Current. The contribution of each forcing factor (e.g., wind) is identified by removing the forcing factor from the control configuration and comparing the mean state of such a configuration with that of the control configuration. The methodology is further discussed in Section 4.1.

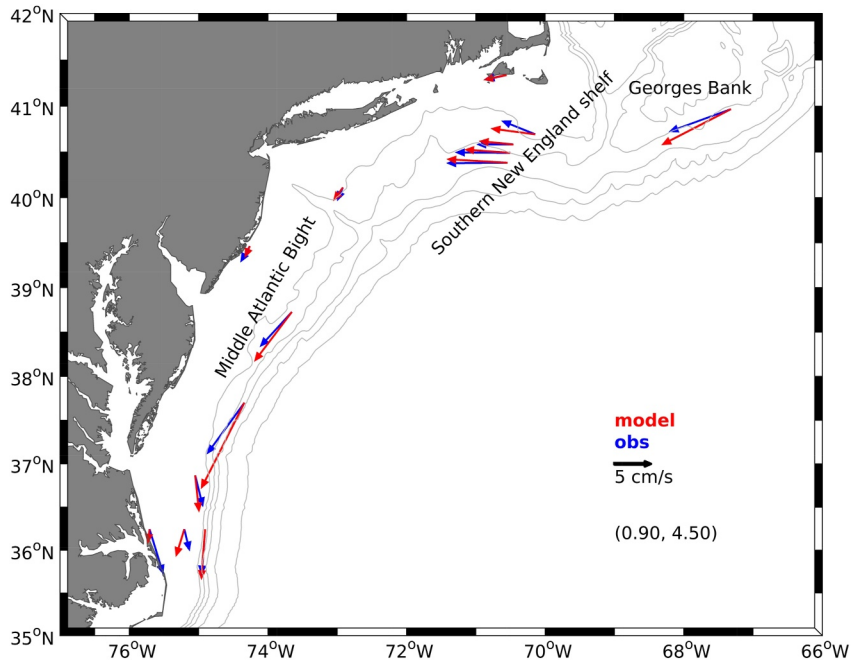

Figure 6. Mean depth-averaged current vectors at locations of long-term observations in the Middle Atlantic Bight. Observations from current meters (Lentz, 2008) are shown in blue, and modeled 2003–2009 averaged currents at the same locations are shown in red. 50-, 70-, 100-, 200-, and 1,000 m isobaths are contoured in gray. The complex correlation coefficients are shown in the parenthesis for amplitude consistency and angle difference (degree).

3. Wind Versus Freshwater Runoff in Driving Shelf Circulation

The climatological simulation reproduces the broad-scale equatorward flows in the entire NWA shelf system (Figures 7a and 8a). On the Labrador Shelf, the coastal current can be identified, along with anti-cyclonic circulation around the banks (e.g., Hamilton Bank at 54°N). To the south, the Scotian Shelf inflow into the GoM, the Maine coastal current, the anti-cyclonic circulation around the Georges Bank (~41°N), and the southward flow in the MAB including the shelfbreak jet are realistically simulated. All of these circulation patterns are consistent with earlier studies (see reviews by Loder et al., 1998; Townsend et al., 2006). The mean circulation is largely consistent with the results of the wind-driven, barotropic (for the shelf) model in YC21. One noticeable difference is the absence of the baroclinic shelfbreak jet in the wind-driven two-layer model (c.f. Figures 5 and Figure 10 in YC21), which does not include buoyancy forcing. Accompanying the mean circulation, the mean sea level on the continental shelves is generally higher along the coast, consistent with the mean along-shelf flow being geostrophic. Latitudinally, the sea level along the Labrador coast is higher, in contrast to the relatively lower sea level from the Scotian Shelf to the MAB. This sets up an along-shelf sea level tilt and thus pressure gradient (Figure 9). The mean sea level gradient along the 30 m isobath from the MAB to the Labrador Shelf (Figure 1) is 3.1×10^{-8} (Table 1), with larger gradients between the Labrador Shelf and the Gulf of St. Lawrence (between 5,500 and 6,000 km) and over the Scotian Shelf (2,000–3,000 km). Over the Labrador Shelf, the along-shelf sea level gradient is 6.1×10^{-8}, whereas from MAB to Scotian Shelf the gradient is 1.8×10^{-8}, comparable to but smaller than 3.7×10^{-8} in (Lentz, 2008) and $3\sim4 \times 10^{-8}$ in YC21. However, the inference in Lentz (2008) is only for the northern MAB and is not isobath specific. Similarly, YC21 focuses on the latitude range of 37°N to 41°N in the MAB and does not follow a specific isobath. The actual sea level gradient along the 30 m isobath in the northern MAB from the NWA model is 1.7×10^{-8}. It is worth noting that there is significant variability of mean sea level gradient in both the along-isobath direction (Figure 9) and the cross-isobath directions (not shown), indicating the necessity of accounting for the spatial heterogeneity of the pressure gradient term and the complexity of accurately measuring this term. The dynamical implications of the along-shelf pressure gradient will be further discussed below.

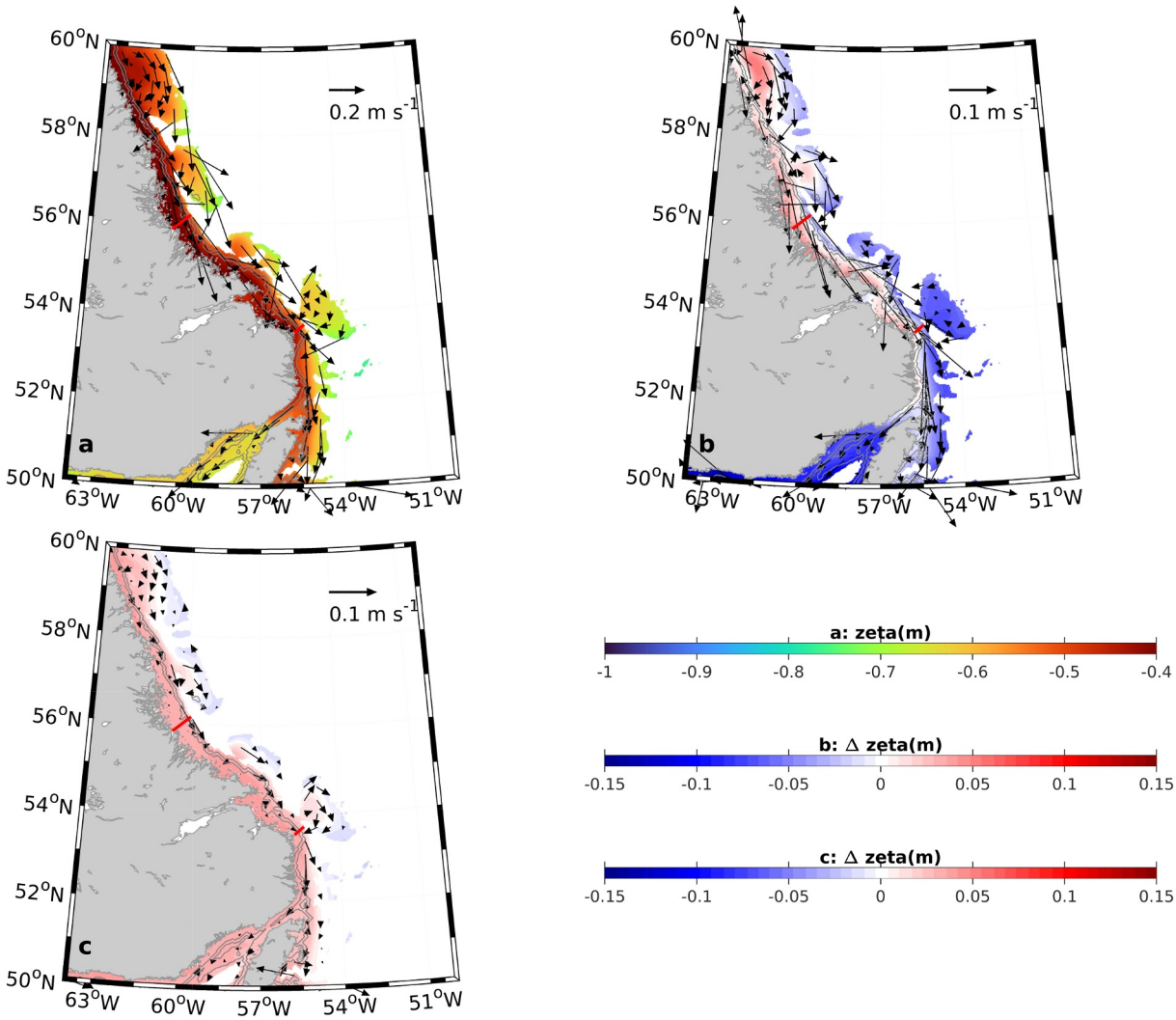

Figure 7. Depth-averaged flow (vectors) and sea surface height (color) on the Labrador Shelf (shallower than 200 m) for the control experiment (a), and the changes between the control experiment and sensitivity experiments: *ctrl-noWind* (b), and *ctrl-noRiv* (c). 50 and 100 m, isobaths are contoured in gray. Locations of two cross-shelf sections are shown in red.

3.1. Responses of the Along-Shelf Flow to Wind and Freshwater Runoff

The relative roles of wind stress forcing and freshwater runoff are elucidated here based on sensitivity experiments without wind stress and freshwater point sources respectively within the model domain. The difference between the control experiment and *noWind* experiment illustrates the contribution of the wind stress within the model domain to the mean shelf circulation, which differs significantly in different regions (Figures 7b and 8b). On the Labrador Shelf, wind stress drives an along-shelf flow along the coast, which is expected as the mean wind stress is largely in the along-shelf direction (Figure 1). Correspondingly, the sea level is higher near the coast than offshore as expected from geostrophy. In contrast, on the southern shelves, the wind-contributed flow is primarily up shelf, in the opposite direction as the mean flow (Figure 8b). In other words, wind is not driving, but rather opposing the equatorward mean flow from the Scotian Shelf to the MAB. This reflects the northeastward mean wind stress, which is against the mean flow and depresses the mean sea level in this sector (Figure 1). The along-shelf sea level gradient is drastically different without wind stress forcing (Figure 9). The overall sea level tilt is largely eliminated with a gradient of 7.5×10^{-9} or one order of magnitude smaller than that of the control experiment. While the sea level along the Labrador Shelf is decreased slightly without wind stress, the change of sea level gradient along the whole NWA segment is primarily a result of the elevated sea level on the southern

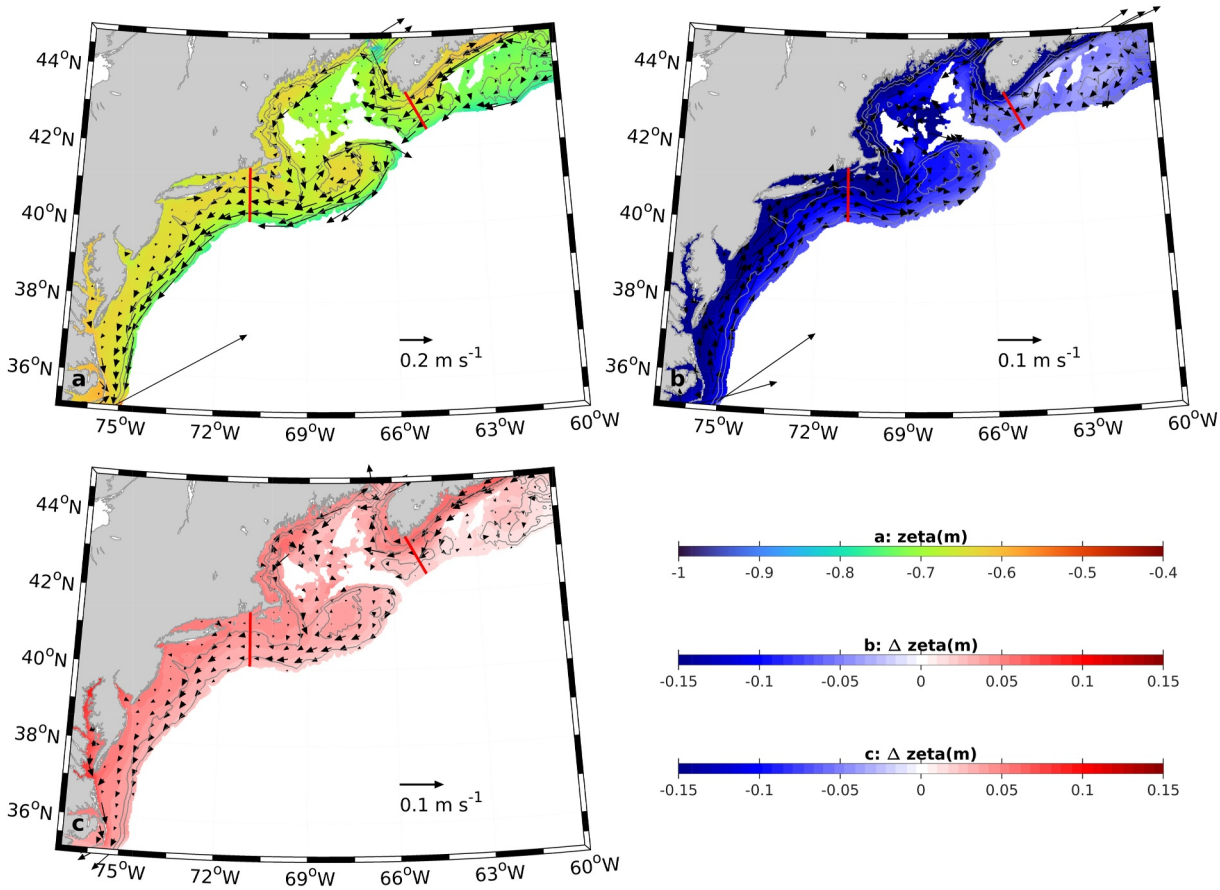

Figure 8. Depth-averaged flow (vectors) and sea surface height (color) on the Scotian Shelf, in the Gulf of Maine and in the Mid-Atlantic Bight (shallower than 200 m) for the control experiment (a), and the changes between the control experiment and sensitivity experiments: *ctrl-noWind* (b), and *ctrl-noRiv* (c). 50 and 100 m isobaths are contoured in gray. Locations of two cross-shelf sections are shown in red. Vector scales in Figures 7a and 7c and Figures 8b and 8c are consistent for comparison purposes.

shelves from the Gulf of St. Lawrence to the MAB: without upwelling-favorable mean wind, the sea level on the southern shelves would rise by ∼0.1–∼0.18 m.

In comparison to wind, the contribution from freshwater runoff to the mean circulation is more consistent. On both the northern and southern shelves, the response of currents to freshwater runoff is in the same direction as the mean flow, despite a smaller magnitude than the wind-driven component (Figure 7c). The response of the coastal sea level to freshwater runoff on the Labrador Shelf is comparable to the wind-driven counterpart, at ∼0.06 m, which is also similar to the response to runoff on the southern shelves (Figure 8c). The largest contribution comes from the St. Lawrence River, elevating the coastal sea level by a maximum of 0.18 m at the source region (Figure 9, ∼4,300 km). Due to the consistent contribution of freshwater runoff, the overall along-shelf sea level gradient on the whole NWA shelf is less sensitive to the presence or absence of continental freshwater input. The sea level tilt without freshwater input is 3.2×10^{-8}, very close to that in the control state.

To further quantify and compare the contributions from wind stress and continental freshwater runoff, the mean along-shelf transports at four cross-shelf sections are examined (Figure 10). The sections span from the coast to the 200 m isobath in the cross-isobath direction at the middle Labrador Shelf, southern Labrador Shelf, Scotian Shelf and northern MAB (Figure 1). The along-shelf transport crossing a section is calculated by utilizing the native model grid points (i.e., no interpolation used) to guarantee volume conservation. The bottom topography on the Labrador Shelf is rugged, with several submarine banks distributed from north to south. For better representation of the mean shelf circulation, the two transects on the Labrador Shelf are located off the rugged topography where the 200 m isobath is relatively straight. The resulting along-shelf transports across the transects thus reflect the Labrador coastal current rather than the upper branch of the Labrador slope current (Lazier &

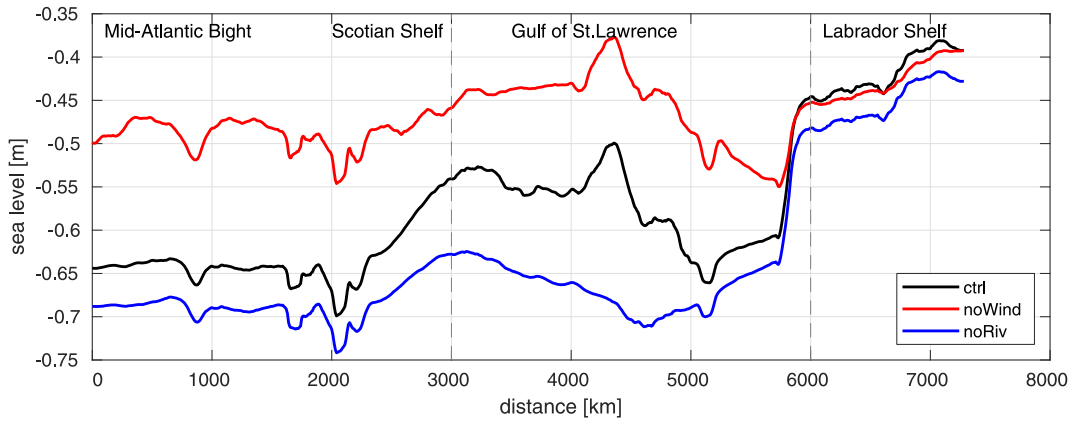

Figure 9. Mean along-isobath (30 m, Figure 1) sea level on the Northwest Atlantic shelf. Results from three experiments are shown: *ctrl* (black), *noWind* (red), and *noRiv* (blue). Variability with a spatial scale less than 100 km is smoothed out. The vertical dashed lines mark the boundaries of three along-isobath segments: Mid-Atlantic Bight to Scotian Shelf (0–3,000 km), Gulf of St. Lawrence (3,000–6,000 km), and Labrador Shelf (6,000–7,280 km).

Wright, 1993). On the southern shelves, the bottom topography is relatively smooth and thus the transports capture the mean flow over the relatively broad shelf. The overall along-shelf transport decreases equatorward, from approximately 1.1–1.2 Sv on the Labrador Shelf to 0.85 Sv in the northern MAB (Figure 10), consistent with earlier estimates (Loder et al., 1998) and the "leaky pipe" concept (Lozier & Gawarkiewicz, 2001). The establishment of such a pattern is mainly attributed to the wind stress forcing. On the Labrador Shelf, the mean wind stress in roughly down coast, accelerating the mean along-shelf current. However, from the Scotian Shelf to the

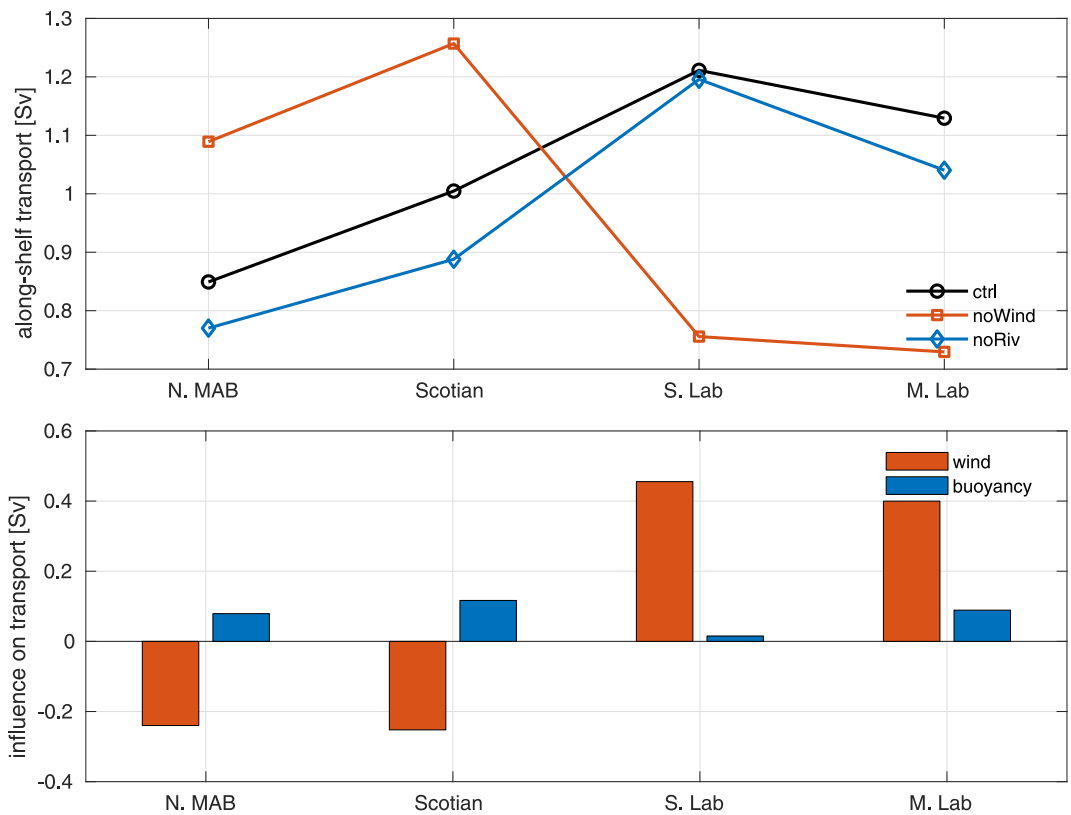

Figure 10. Upper panel: along-shelf transport at the four cross-shelf sections from three experiments: *ctrl* (black circle), *noWind* (red square), and *noRiver* (blue diamond). Transport is integrated from surface to bottom, from the coast to 200 m isobath. Lower panel: the influence of wind (*ctrl-noWind*) and buoyancy (*ctrl-noRiv*) on the along-shelf transport.

Table 1
Along-Isobath Sea Level Gradient Based on Linear Fitting for the Whole Segment (0–7,280 km), Mid-Atlantic Bight (MAB) to Scotian Shelf (0–3,000 km) and Labrador Shelf (6,000–7,280 km)

	Whole segment	MAB—Scotian	Labrador
ctrl	3.1×10^{-8}	1.8×10^{-8}	6.1×10^{-8}
noWind	7.5×10^{-9}	1.4×10^{-10}	5.9×10^{-8}
noRiv	3.2×10^{-8}	9.1×10^{-9}	6.1×10^{-8}

MAB, the mean wind stress is up coast, against the mean flow. Without wind stress, the along-shelf transport would be significantly reduced to 0.7∼0.8 Sv on the Labrador shelf and increased to 1.1∼1.2 Sv on the Scotian Shelf and in the MAB (Figure 10). This would completely change the main characteristic of the along-shelf transport being a "leaky" system. In comparison, the response of the along-shelf transport to continental runoff is less significant, although freshwater discharge consistently contributes to the mean equatorward along-shelf flow (Figure 10). Specifically, on the Labrador Shelf, wind stress is the dominant driver of along-shelf transport, more so than the freshwater runoff. On the southern shelves downstream of the Gulf of St. Lawrence, freshwater runoff is clearly important in driving the mean equatorward shelf flow. Even so, the influence of wind stress (i.e., magnitude of change in transport with vs. without the forcing factor) is still larger than the influence of runoff. Therefore, from a holistic view, wind is more influential on the mean along-shelf transport. However, it is also worth noting the non-closure nature of the transport quantification, which is by no means a budget calculation. This is because wind stress and freshwater runoff are not the only two drivers of the shelf circulation: there are additional forcing processes that also contribute to the shelf water transport. A difficulty in partitioning the contributions is that interactions of wind-driven and runoff-driven processes are nonlinear. These aspects will be discussed in Section 4.1.

3.2. Circulation Dynamics

To better understand the responses of the along-shelf flow to wind stress and freshwater runoff, simplified shelf circulation dynamics are considered. Setting the positive x direction as cross-shelf (Note: Cross-shelf (along-shelf) and cross-isobath (along-isobath) are equivalent terms and are used interchangeably in this paper) pointing offshore, positive y direction as along-shelf pointing poleward, and z-axis positive upward, the governing equations for the mean cross- and along-shelf momentum, are:

$$\vec{U} \cdot \nabla u - fv = -\frac{1}{\rho_0}\frac{\partial p}{\partial x} + \frac{1}{\rho_0}\frac{\partial \tau^x}{\partial z} \tag{1}$$

$$\vec{U} \cdot \nabla v + fu = -\frac{1}{\rho_0}\frac{\partial p}{\partial y} + \frac{1}{\rho_0}\frac{\partial \tau^y}{\partial z} \tag{2}$$

where $\vec{U} \equiv (u,v,w)$ is the velocity vector, f is the Coriolis parameter, ρ_0 is the mean shelf water density, p is the pressure field, and τ is the total stress, with superscript x and y denoting its components in the cross- and along-shelf directions. In the cross-shelf direction, the pressure gradient term largely balances the Coriolis term (Figures 11a–11d), that is, the along-shelf flow is largely geostrophic. The relatively minor imbalance is due to the nonlinear advection term, mostly in nearshore regions and where the topography is irregular. With this information, Equation 1 can be simplified as:

$$v \approx \frac{1}{f\rho_0}\frac{\partial p}{\partial x} \tag{3}$$

or in the form of thermal-wind balance:

$$\frac{\partial v}{\partial z} \approx -\frac{g}{f\rho_0}\frac{\partial \rho}{\partial x} \tag{4}$$

where the g is gravitational acceleration.

Vertically integrating Equation 4 from the ocean bottom gives the along-shelf velocity in terms of bottom velocity v_{bot} and the cross-shelf density gradient:

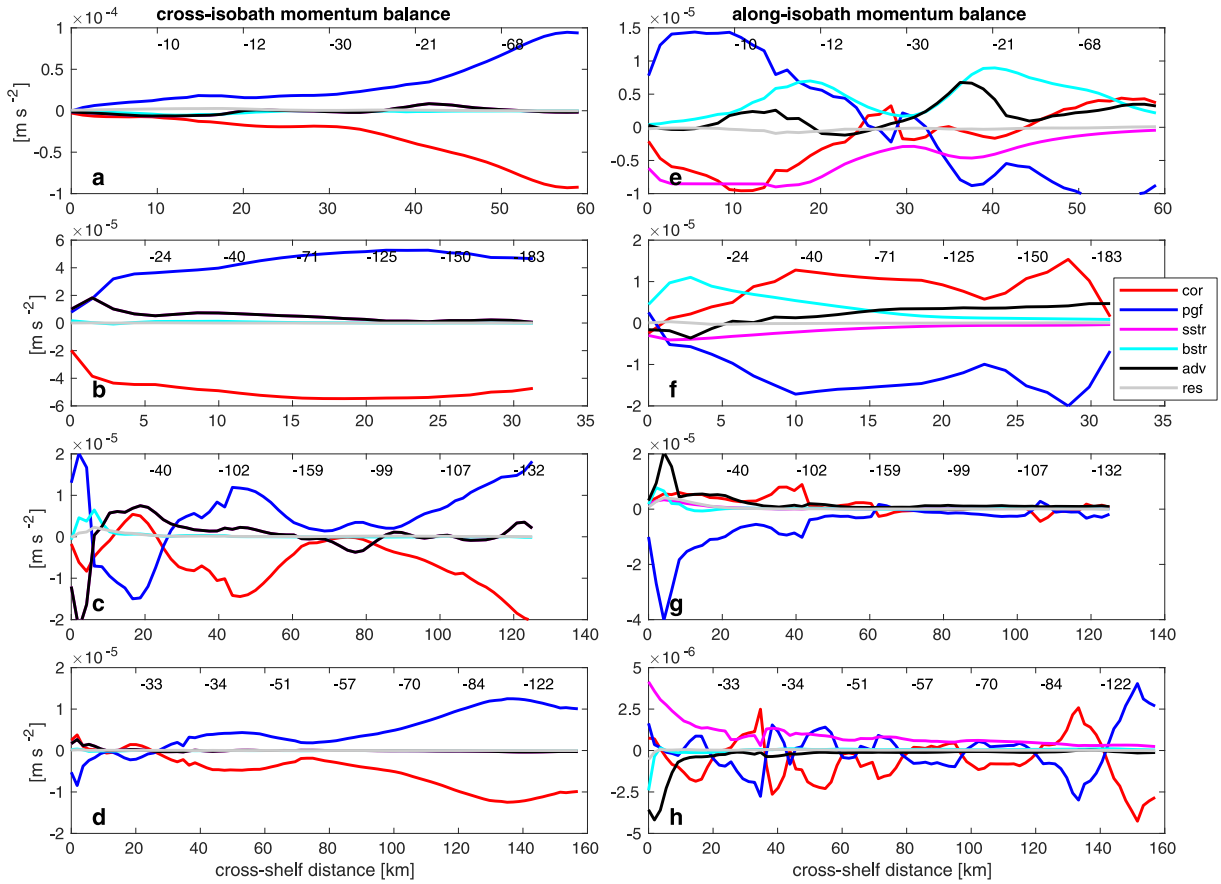

Figure 11. Depth-averaged cross-isobath momentum balance (a, b, c, d) and along-isobath momentum balance (e, f, g, h) at middle Labrador section (a, e), southern Labrador section (b, f), Scotian Shelf section (c, g) and northern Mid-Atlantic Bight section (d, h). Corioils (cor), pressure gradient force (pgf), wind stress (sstr), bottom stress (bstr), nonlinear advection (adv), and residual terms (unit: m s^{-2}) are shown. *X*-axis is the cross-shelf distance from the coast with corresponding water depth (unit: meter) shown on the top of each panel. Each term is decomposed to along-isobath and cross-isobath components according to the local orientation of the isobath.

$$v = v_{bot} - \frac{g}{f\rho_0}\int_{-h}^{z}\frac{\partial \rho}{\partial x}dz' \tag{5}$$

Therefore, the depth-averaged shelf flow is:

$$v_{da} = v_{bot} - \frac{g}{\rho_0 f h}\int_{-h}^{0}\int_{-h}^{z}\frac{\partial \rho}{\partial x}dz'dz \tag{6}$$

So, the depth-averaged along-shelf velocity is determined by the along-shelf bottom velocity and the (depth-averaged, cumulative) cross-shelf density/buoyancy gradient. The former reflects the barotropic property of the along-shelf flow, and the latter represents the baroclinic part. To understand the along-shelf bottom flow, consider the along-shelf momentum balance Equation 2. Denoting the nonlinear advection term as $A_y = -\vec{U}\cdot\nabla v$, and Coriolis term $C_y = -fu$, Equation 2 becomes:

$$0 = -\frac{1}{\rho_0}\frac{\partial p}{\partial y} + \frac{1}{\rho_0}\frac{\partial \tau^y}{\partial z} + A_y + C_y \tag{7}$$

Depth-integration gives:

$$0 = -\frac{1}{\rho_0}\int_{-h}^{0}\frac{\partial p}{\partial y}dz + \frac{1}{\rho_0}(\tau^{sy} - \tau^{by}) + \int_{-h}^{0}A_y dz + \int_{-h}^{0}C_y dz \quad (8)$$

where τ^{sy} and τ^{by} are wind stress and bottom stress. In 2-D, linear shelf models that do not consider the variation in the along-shelf direction (i.e., straight coastline, $\frac{\partial}{\partial y} = 0$, except for the along-shelf pressure gradient term), the last two terms in Equation 8 are zero, simply because there is no cross-shelf transport at the coast and no volume divergence in the cross-shelf direction. In such a case, Equation 8 is reduced to:

$$0 = -\frac{1}{\rho_0}\int_{-h}^{0}\frac{\partial p}{\partial y}dz + \frac{1}{\rho_0}(\tau^{sy} - \tau^{by}) \quad (9)$$

That is, the along-shelf pressure gradient term is balanced by the term of stress difference in the along-shelf direction. This is the fundamental argument in earlier 2D shelf models (e.g., Csanady, 1976; Lentz, 2008; Stommel & Leetmaa, 1972). However, such a simple balance does not always hold for 3-D models with realistic coastline and bathymetry (Figures 11e–11h).

Unlike in 2-D shelf models, the mean shelf flow in a 3-D model does not necessarily follow the local isobath, which leads to a non-zero Coriolis term in the along-shelf (along-isobath) direction. For example, the negative and positive Coriolis term along the middle Labrador transect reflects flow convergence as a result of offshore flow on the inner shelf and onshore flow on the outer shelf (Figure 11e). Similarly, the positive Coriolis term along the southern Labrador transect suggests that the depth-averaged flow at this location has a significant onshore component (Figure 11f). The offshore/onshore cross-isobath flow at these two locations presumably reveals the contribution of the cross-shelf flow to the along-shelf transport, which is larger at the southern Labrador Shelf (Figure 10). In the northern MAB, the cross-isobath component of the depth-averaged shelf flow is more complex, resulting in an alternating positive/negative Coriolis term (Figure 11h). Another factor leading to the departure from Equation 9 is the non-negligible nonlinear advection term, which is particularly large on the Labrador Shelf and over the inner Scotian Shelf and MAB (Figures 11e–11h).

Perhaps the most noteworthy result is the variability of the along-shelf pressure gradient term, which is clearly not spatially uniform. On the outer part of the middle Labrador section, negative pressure gradient force (equatorward) corresponds to equatorward flow at the shelfbreak (Figures 12a). Along with equatorward wind stress, the pressure gradient force balances bottom stress, Coriolis, and nonlinear advection terms. The momentum balance differs significantly at the shallower part of the middle Labrador shelf as the pressure gradient term reverses direction (Figure 11e). On the south Labrador shelf, the along-shelf pressure gradient term is consistent, largely balancing the Coriolis, advection, and bottom stress terms (Figure 11f). At this location, the equatorward pressure gradient term is associated with the well-defined along-shelf flow (Figure 12d), supporting the notion that along-shelf pressure gradient is key in driving the mean shelf flow. On the Scotian Shelf, the pressure gradient term is mostly equatorward and is particularly large near the coast (Figure 11g). At locations of equatorward flow (e.g., around 50 km from the coast, Figure 12g), the pressure gradient term is the leading term in the along-shelf momentum balance. In the northern MAB, the along-shelf pressure gradient term is much more complicated (Figure 11h). The mean equatorward shelfbreak jet and along-shelf flow are well represented (Figure 12j). However, the major momentum balance in the along-shelf direction clearly departs from the 2-D framework described in Equation 9. The overall balance is between the poleward wind stress and pressure gradient force and Coriolis terms, the latter two alternate signs in the cross-shelf direction. As the along-isobath pressure gradient force is determined by both along-isobath sea level tilt and density gradient, the alternating pressure gradient term in the northern MAB represents the complex co-working of both barotropic and baroclinic processes in this region.

The complex dynamics of along-shelf momentum balance require a more complete consideration of the terms controlling the along-shelf flow including the along-shelf bottom velocity, which is related to bottom stress, regardless of linear or quadratic drag law. The bottom stress can be retrieved from Equation 8:

$$\tau^{by} = \tau^{sy} + \rho_0\left(\int_{-h}^{0}P_y dz + \int_{-h}^{0}A_y dz + \int_{-h}^{0}C_y dz\right) \quad (10)$$

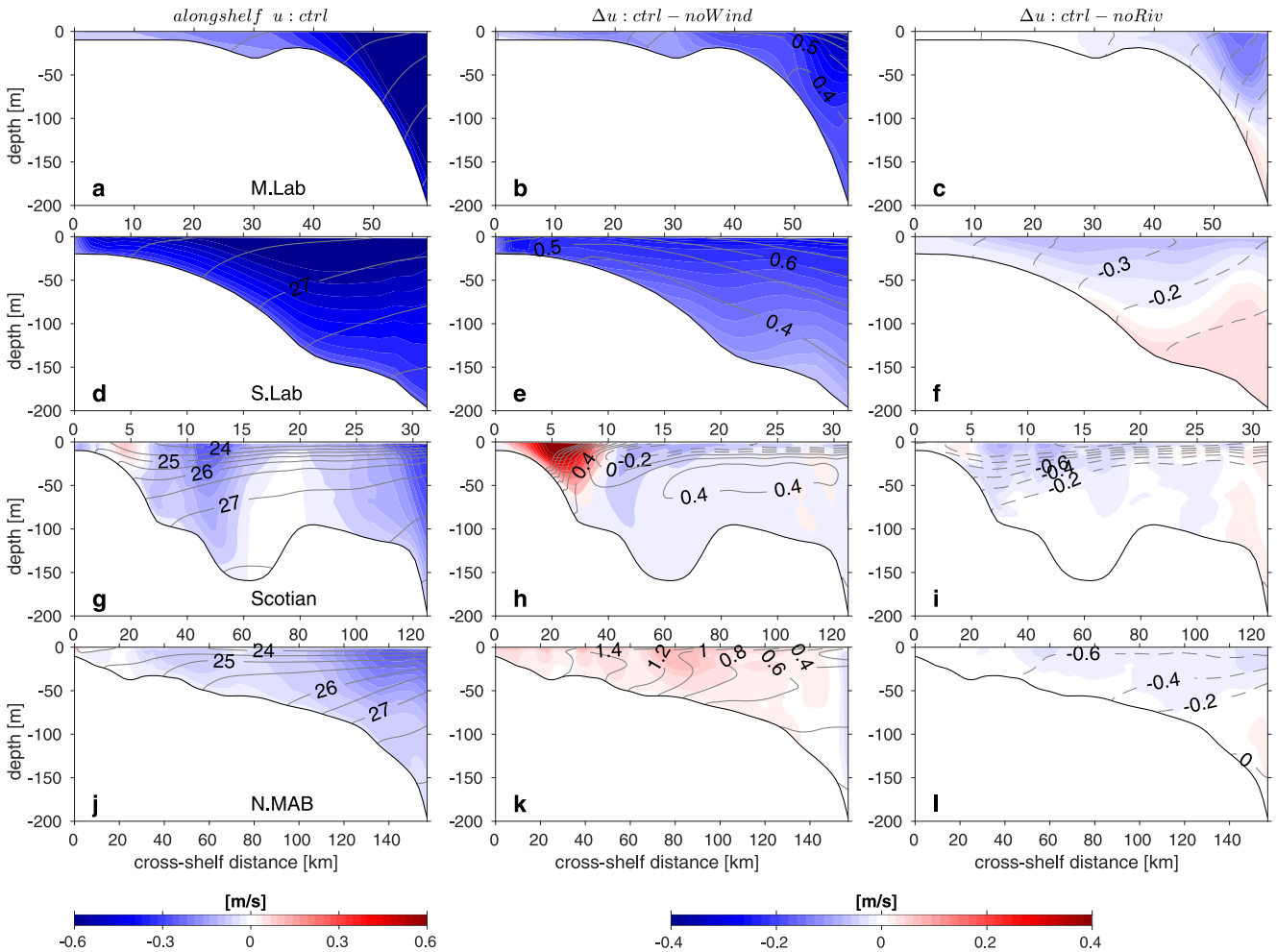

Figure 12. Along-isobath velocity with cross-shelf density field at four cross-sections: middle Labrador, southern Labrador, Scotian Shelf, and northern Mid-Atlantic Bight. Velocity is rotated to along-isobath direction according to the local orientation of the isobath. The results from the *ctrl* experiment are shown in the first column (a, d, g, j), with density C.I. 0.5 kg m^{-3}. The changes between the control and *noWind* experiment are shown in the second column (b, e, h, k). The changes between the *ctrl* and *noRiv* experiment are shown in the third column (c, f, i, l). The C.I. for density anomaly is 0.1 kg m^{-3} for panels (b, c, e, f), and 0.2 kg m^{-3} for panels (h, i, k, l). Solid (dashed) contours represent density increase (decrease).

where $P_y = -\frac{1}{\rho_0}\frac{\partial p}{\partial y}$

Using linear bottom drag law, the mean bottom velocity can be estimated as:

$$v_{bot} = \frac{\tau^{by}}{\rho_0 r} = \frac{1}{r}\left(\frac{\tau^{sy}}{\rho_0} + \int_{-h}^{0} P_y dz + \int_{-h}^{0} A_y dz + \int_{-h}^{0} C_y dz\right) \tag{11}$$

can be rewritten as:

$$v_{bot} = \frac{\tau^{by}}{\rho_0 r} = \frac{1}{r}\left(\frac{\tau^{sy}}{\rho_0} - gh\frac{\partial \eta}{\partial y} - \int_{-h}^{0}\int_{z}^{0}\frac{1}{\rho_0}\frac{\partial \rho}{\partial y} g dz' dz + \int_{-h}^{0} A_y dz + \int_{-h}^{0} C_y dz\right) \tag{12}$$

Or

$$v_{bot} = \frac{\tau^{by}}{\rho_0 r} = \frac{1}{r}\left(\frac{\tau^{sy}}{\rho_0} - gh\frac{\partial \eta}{\partial y} + \left(\int_{-h}^{0} P_y dz - \left(-gh\frac{\partial \eta}{\partial y}\right)\right) + \int_{-h}^{0} A_y dz + \int_{-h}^{0} C_y dz\right) \tag{13}$$

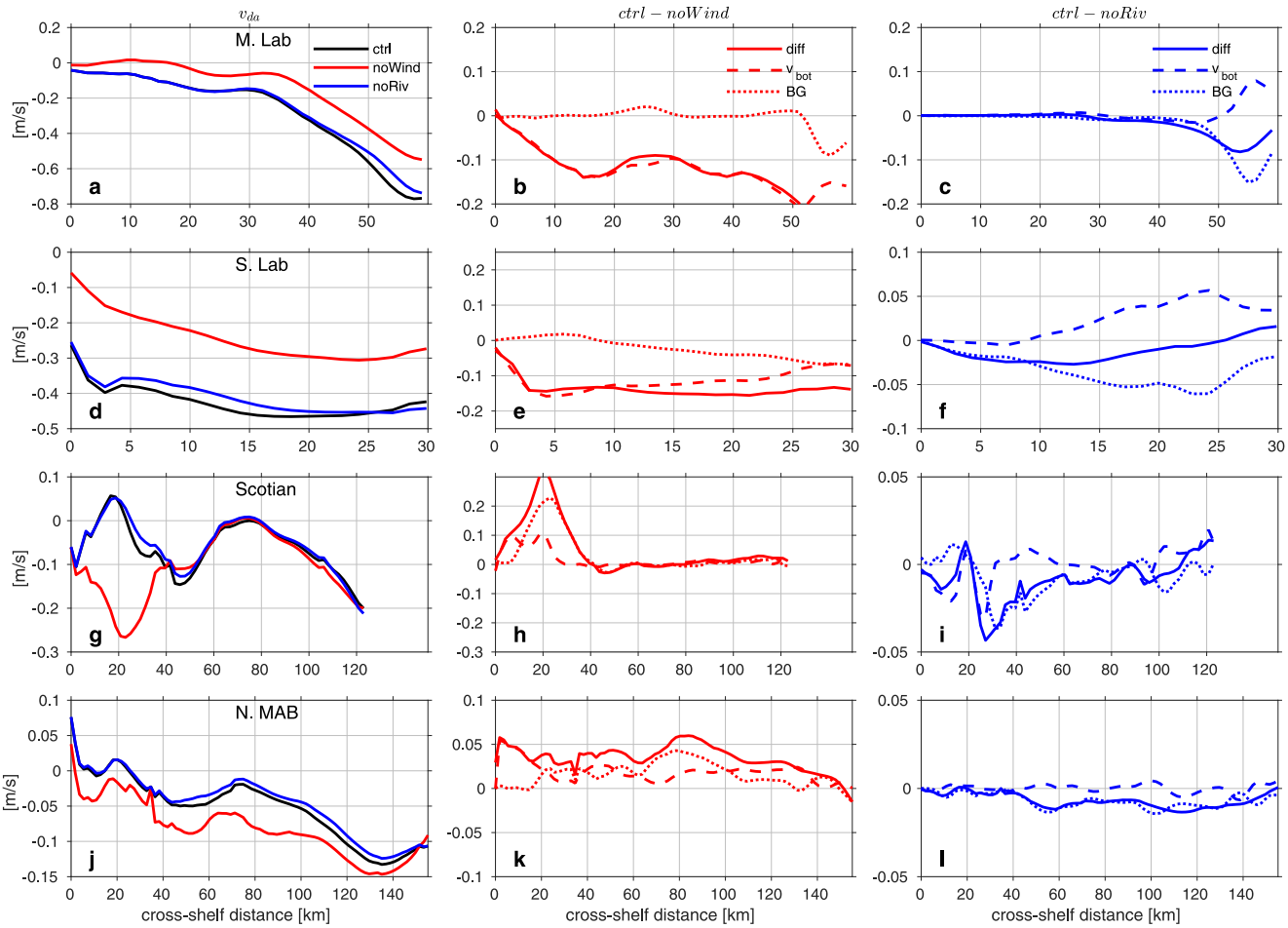

Figure 13. Depth-averaged along-isobath velocity at the middle Labrador section (a), southern Labrador section (d), Scotian Shelf section (g) and northern Mid-Atlantic Bight section (j). Each term is rotated to along-isobath direction according to the local orientation of the isobath. Results from *ctrl*, *noWind*, and *noRiv* experiments are shown in black, red, and blue, respectively. The changes of depth-averaged velocity from the *noWind* experiment at each section are shown in panels (b, e, h, and k). Similarly, the results from the *noRiv* experiment are shown in panels (c, f, i, l). The total change term is plotted in solid lines, the change of bottom velocity (v_{bot}) is plotted in dashed lines, and the changes of buoyancy gradient term (BG) is plotted in dotted lines (Equation 6).

In other words, the along-shelf bottom velocity is determined by the along-shelf wind stress $\frac{\tau^{sy}}{\rho_0}$, barotropic along-shelf pressure gradient term or the along-shelf sea level tilt term $-gh\frac{\partial \eta}{\partial y}$, baroclinic pressure gradient term $-\int_{-h}^{0}\int_{z}^{0}\frac{1}{\rho_0}\frac{\partial \rho}{\partial y}g dz' dz$, nonlinear advection term $\int_{-h}^{0}A_y dz$, and Coriolis term $\int_{-h}^{0}C_y dz$ due to cross-shelf flow. Again, the depth-averaged cross-shelf flow is not necessarily zero and this last term cannot be ignored. If instead using quadratic drag formulation, which is the case in the primitive-equation NWA model, it would be very difficult to infer the mean bottom velocity in such a diagnostic calculation using mean stress terms due to the nonlinear formulation. Nevertheless, without necessarily knowing the linear drag coefficient, different terms controlling the mean bottom velocity can be compared against each other based on Equation 13.

3.3. Governing Terms of the Wind-Driven and Runoff-Driven Along-Shelf Flow

Both wind stress and freshwater runoff contribute to the equatorward mean flow over the NWA shelf; however, the associated processes differ considerably. On the Labrador Shelf, a significant portion of the along-shelf flow is wind-driven contribution, which exists through the entire water column (Figures 12b and 12e). The depth-averaged wind-driven component is larger than 0.1 m s^{-1}, consistently across the middle and southern Labrador sections (Figures 13a and 13d). The strong along-shelf wind also moves denser Labrador slope water toward the coast, setting up a cross-shelf density gradient, particularly at the outer shelf (Figures 12b and 12e). Such a setup would enhance the vertical shear of the along-shelf velocity according to thermal-wind balance

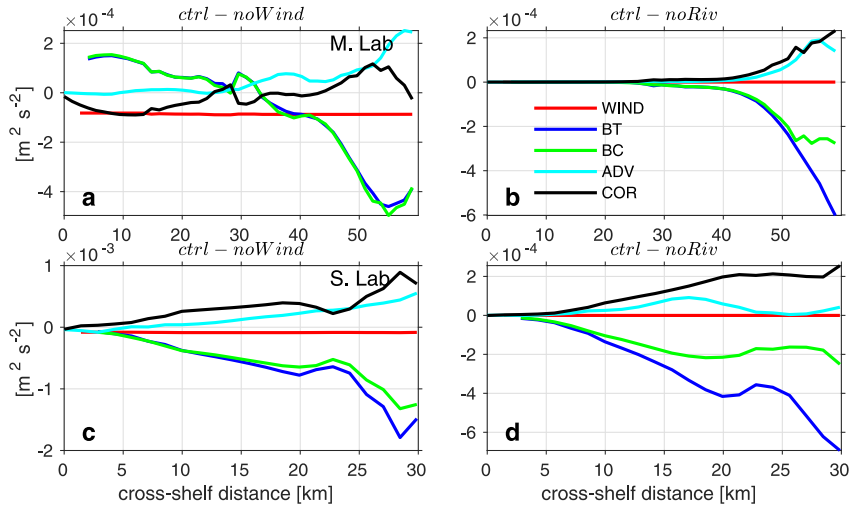

Figure 14. Dynamical terms (Equation 13, unit $m^2\ s^{-2}$) controlling the mean along-isobath bottom velocity at mid-Labrador section (a–b), and south Labrador section (c–d). Each term is rotated to along-isobath direction according to the local orientation of the isobath. The differences between the *ctrl* experiment and *noWind* experiment are shown in the first column (a, c); The differences from *noRiv* experiment are shown in the second column (b, d). Contributions from wind stress (WIND), barotropic pressure gradient (BT), baroclinic pressure gradient (BC), advection (ADV), and Coriolis (COR) terms are color coded in each panel.

(Equation 4). The combination of enhanced shear with wind-forced equatorward bottom velocity determines the strength of the depth-averaged flow and thus along-shelf transport. Diagnostic calculation shows that the contribution of wind stress to the mean along-shelf flow is primarily through the wind-driven along-shelf bottom velocity and, to a much less degree, the cross-shelf density gradient (Equation 6 and Figures 13b and 13e). In other words, the wind-driven flow on the Labrador Shelf is largely barotropic. Indeed, among the terms controlling the along-shelf bottom velocity, wind stress term is consistently down shelf (i.e., equatorward) (Figures 14a and 14c).

In comparison to the wind-driven component, the contribution of freshwater runoff to the along-shelf flow on the Labrador Shelf is less significant. The equatorward flow resulting from freshwater runoff is significant in areas where the cross-shelf density gradient is large: the outer shelf at the middle Labrador section and the inner to middle shelf at the southern Labrador section (Figures 12c and 12f). The resulting depth-averaged contribution is up to ∼0.08 m s^{-1}, less than the wind-driven counterpart, and is less consistent across the entire section. Another difference is that the equatorward flow driven by freshwater runoff is predominantly balanced by the cross-shelf density gradient (Figures 13c and 13f) stemming from the freshwater input, leading to larger horizontal density gradients than the wind-driven counterpart. The larger density gradient and thus stronger vertical shear of along-shelf velocity is also consistent with the poleward flow anomaly at the bottom (Figures 12c and 12f). Further decomposition of the along-shelf bottom velocity shows that the Coriolis and nonlinear advection terms are responsible for the poleward bottom velocity anomaly at the outer shelf at both the middle and southern Labrador sections (Figures 14b and 14d).

On the Scotian and northern MAB shelves, because the mean wind stress is against the mean shelf flow, removing wind would generally increase the depth-averaged flow. While the response is more coherent across the entire northern MAB section, the wind-forced along-shelf flow is most notable close to the coast over the Scotian Shelf (Figures 12h and 12k). Such a response is determined by both the bottom velocity and cross-shelf density gradient. Upwelling-favorable wind brings denser offshore water toward the coast, creating a larger density increase nearshore. The resultant density anomaly field weakens the existing thermal wind shear and favors a poleward along-shelf flow at 0 ∼ 40 km (Figure 12h). The influence of wind stress on along-shelf bottom velocity is also present, but is less dominant in comparison to that on the Labrador Shelf. The elevated contribution from the cross-shelf density gradient term here is associated with stronger stratification and a larger density gradient between the shelf water and slope water on the southern shelves than that on the Labrador Shelf (compare density contours in Figures 12g and 12j to Figures 12a and 12d), enabling a more effective setup of cross-shelf density gradient by wind-driven circulation. The contribution of freshwater runoff to the mean along-shelf flow on the

Scotian and MAB shelves shares similarities with that on the Labrador Shelves. Freshwater runoff consistently contributes to the equatorward mean flow, although the magnitude is not as large as the wind-driven counterpart. The runoff-forced equatorward along-shelf flow is achieved primary through the setup of the cross-shelf density gradient (Figures 13i and 13l).

4. Discussions

4.1. The Partition of the Contributing Factors to Along-Shelf Transport

As stated in Section 3, quantification and partition of the along-shelf transport are not a budget closure problem: the along-shelf transport in the control experiment is not a linear addition of contributions from wind (*ctrl-noWind*) and runoff (*ctrl-noRiv*) forcing (Figure 10). This is because wind stress and freshwater runoff are not necessarily the only two drivers of the along-shelf flow. Additional forcing mechanisms may also contribute to the along-shelf transport. In addition, interactions between different processes may also affect the mean circulation on the NWA shelf. For example, freshwater discharge would increase the shelf water stratification and along-shelf/cross-shelf density gradients, which could affect the participation of barotropic and baroclinic components in the wind-driven flow. A stronger density gradient could increase the thermal-wind shear of the wind-driven geostrophic flow and thereby reduce the bottom geostrophic velocity. This in turn would reduce the bottom stress and thus increase the net wind-driven transport. In other words, the interaction of wind stress and freshwater runoff can produce a stronger along-shelf flow than the linear addition of the flows separately driven by each process alone. Another aspect to consider is the indirect contributions from the large-scale wind stress field. In the *noWind* experiment, winds from the adjacent open ocean are also removed, which would result in changes in the offshore regions. The changes in the open ocean may also contribute to the responses of shelf circulation, although local winds on the shelves have been shown to be more important (e.g., Yang & Chen, 2021).

To better understand the partition of the transport and the above-mentioned factors, it may be useful to simplify the contributions to the along-shelf transport in the numerical experiments as follows:

$$T_{ctrl} = T_W + T_R + T_{WR} + T_F + T_{FW} + T_{FR} \tag{14}$$

$$T_{noWind} = T_R + T_F + T_{FR} \tag{15}$$

$$T_{noRiv} = T_W + T_F + T_{FW} \tag{16}$$

where T_{ctrl}, T_{noWind}, and T_{noRiv} represent along-shelf transports in the experiments *ctrl*, *noWind*, and *noRiv*; T_W, T_R, and T_{WR} represent the contributions to the total along-shelf transport from wind stress, freshwater runoff, and the interaction between the two, respectively; T_F, T_{FW} and T_{FR} represent the contributions from forcing factors beyond what have been discussed and their interactions with wind stress and freshwater runoff. The individual T_{FW} and T_{FR} terms could be zero, which in such a case means the particular forcing factor does not directly interact with wind or runoff forcing. The differences between the transports in the control and sensitivity experiments represent the contributions from the wind stress and freshwater runoff:

$$\Delta T_{ctrl-noWind} = T_{ctrl} - T_{noWind} = T_W + T_{WR} + T_{FW} \tag{17}$$

$$\Delta T_{ctrl-noRiv} = T_{ctrl} - T_{noRiv} = T_R + T_{WR} + T_{FR} \tag{18}$$

$\Delta T_{ctrl-noWind}$ ($\Delta T_{ctrl-noRiv}$) includes the linear contribution to the along-shelf transport from wind stress (freshwater runoff) forcing as well as contributions resulting from the interaction between the wind stress (freshwater runoff) and additional forcing factors. Holistically, $\Delta T_{ctrl-noWind}$ ($\Delta T_{ctrl-noRiv}$) describes the importance of wind stress (freshwater runoff) in driving the along-shelf transport.

One consistent result at all four cross-shelf sections is that the transport differences between the control and the two sensitivity experiments do not add up to the transport in the control experiment, that is, $T_{ctrl} > \Delta T_{ctrl-noWind} + \Delta T_{ctrl-noRiv}$. Utilizing Equations 14, 17, and 18, one gets $T_F > T_{WR}$. This means that there are additional forcing processes that are important for the along-shelf transport. One obvious candidate is the sub-Arctic inflow from higher latitude.

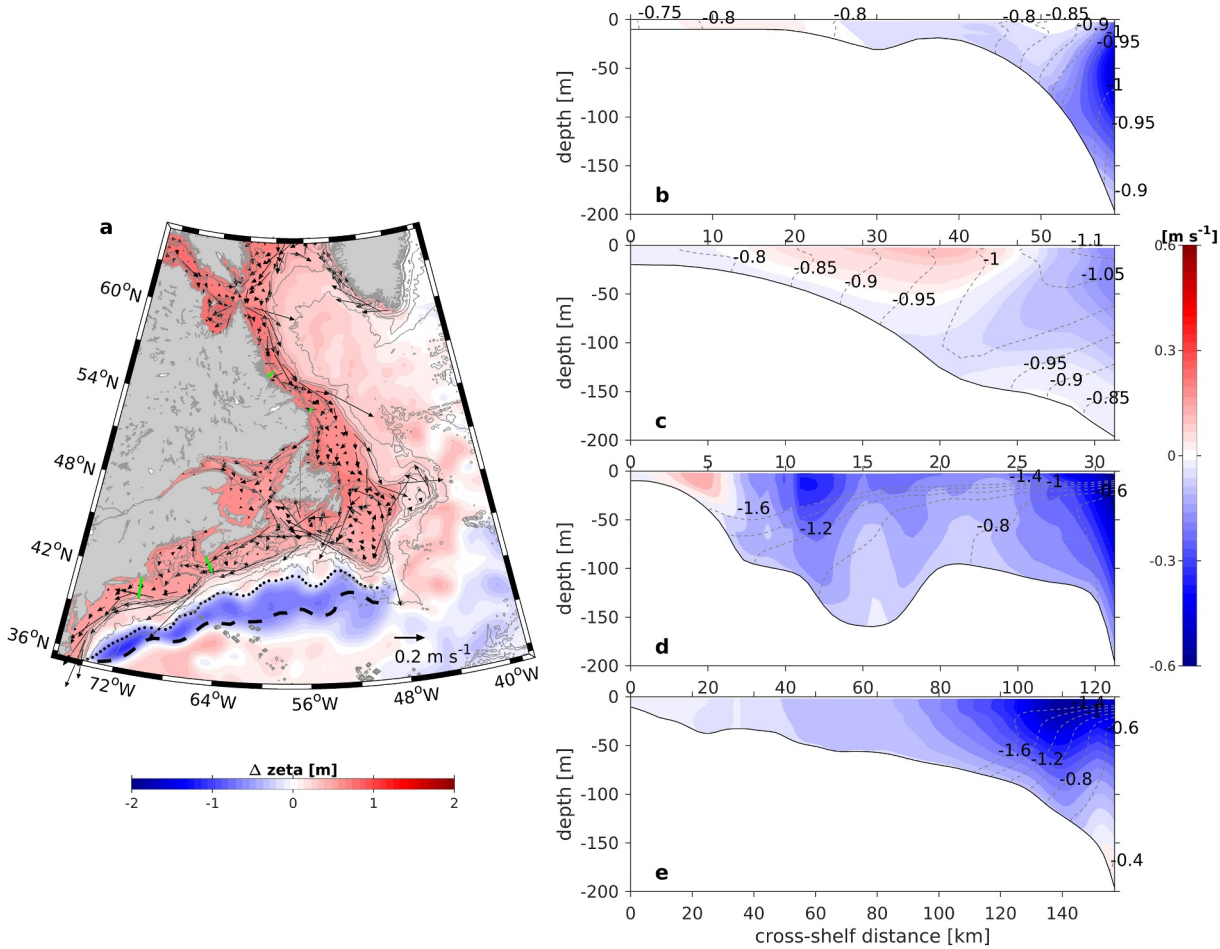

Figure 15. (a) Changes of depth-averaged currents (vectors) and sea surface height (color) between the *ctrl* and *closed* experiments (*ctrl-closed*). (b) Differences (*ctrl-closed*) of along-shelf flow (color) and density field at the four cross-sections (green segments in panel (a). The C.I. for density anomaly is 0.05 kg m^{-3} for panels (b–c) and 0.2 kg m^{-3} for panels (d–e). The dashed (dotted) line represents the Gulf Stream position (15° isotherm at 200 m) in the *ctrl* (*closed*) experiment.

4.2. Other Potential Drivers: Sub-Arctic Inflow

While the roles of wind stress and continental freshwater runoff in driving the along-shelf flow have been elucidated, the contribution of the sub-Arctic inflow from higher latitude needs to be discussed. This is because the NWA shelf flow is inevitably influenced by the subarctic circulation such as Baffin current along the western side of the Davis Strait, along with Greenland coastal currents.

To understand the contribution from the sub-Arctic inflow, particularly the Greenland and Baffin Currents, an additional numerical experiment "*closed*" is conducted. The difference between the steady states of the control experiment and this altered configuration (control run minus closed run or *ctrl-closed*, Figure 15) highlights the roles of the larger-scale sub-Arctic inflow in driving the mean circulation on the NWA shelf.

As expected, the inflow (including sub-Arctic coastal currents) has considerable influence on the mean sea level and circulation. A large portion of the equatorward flow on the NWA shelf can be traced upstream from the along-isobath flow from Baffin Bay (Figure 15a), with contribution from the Greenland Currents, which circulate cyclonically in Baffin Bay (Münchow et al., 2015; Tang et al., 2004). On the Labrador shelf, the continuation of the sub-Arctic inflow is centered at the shelfbreak and brings relatively lighter water with it. The resultant alteration of the density is also centered at the shelfbreak, effectively reducing the lateral density gradient (Figures 12a and 12d vs. Figures 15b and 15c). The weakened density gradient is accompanied by a weakened along-shelf flow over the shallow part of the shelf, consistent with the thermal wind balance. As a result, the

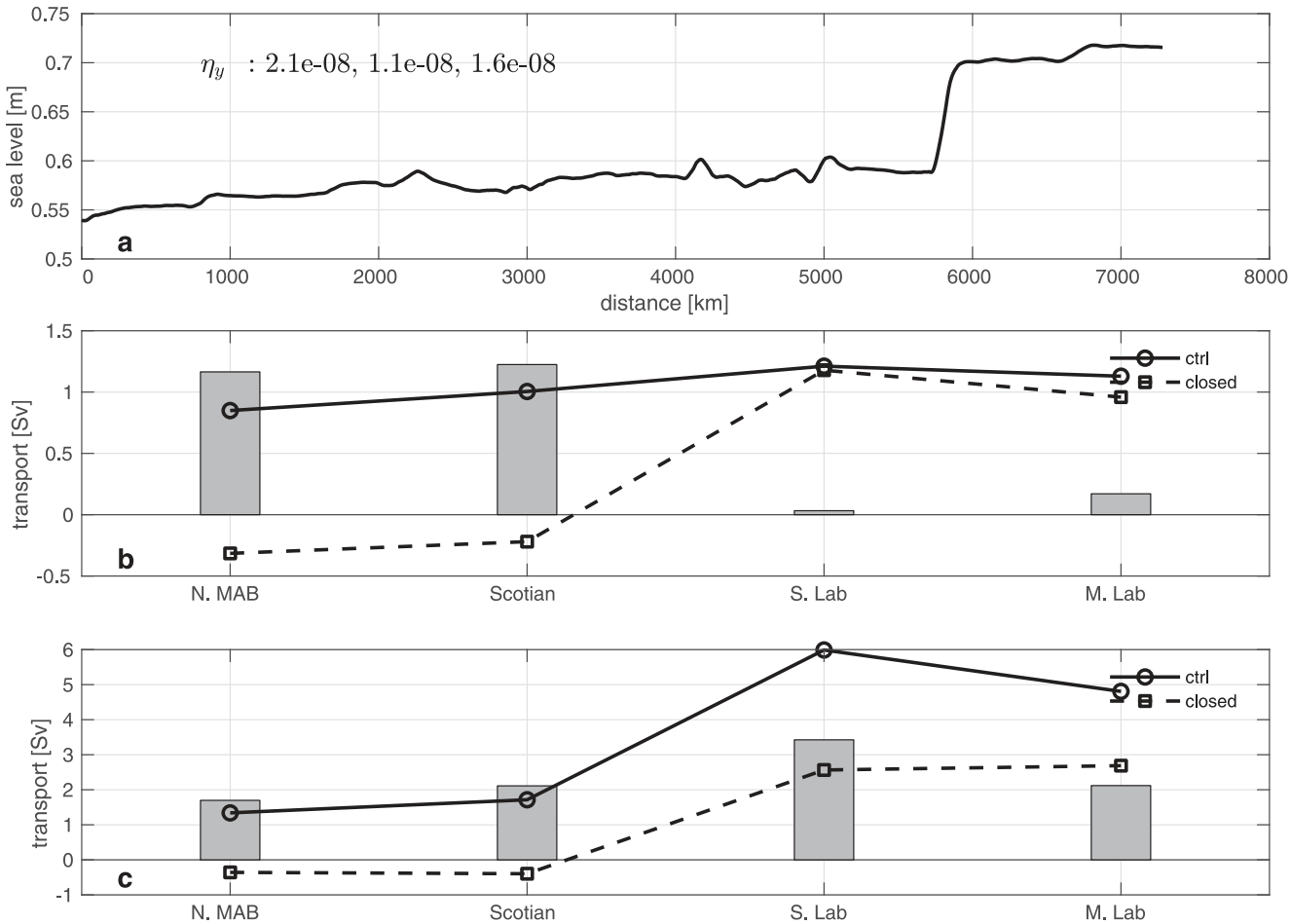

Figure 16. (a) Along-isobath (30 m) sea level change between the *ctrl* and *closed* experiments (*ctrl-closed*). Three sets of along-isobath sea level gradient based on linear fitting for the whole segment (0–7,280 km), Mid-Atlantic Bight to Scotian Shelf (0–3,000 km), and Labrador Shelf (6,000–7,280 km) are shown. (b) Along-shelf transport (0–200 m isobath) at the four cross-shelf sections from the *ctrl* (black circles) and *closed (gray squares)* experiments. Changes of transport (*ctrl-closed*) are shown in light gray bars. (c) Same as panel (b) but for along-shelf transport integrated from 0 to 500 m isobath.

overall contribution from the sub-Arctic inflow to the along-shelf transport at the Labrador shelf is less than 0.2 Sv (Figure 16), smaller than the wind-driven contribution.

The influence of sub-Arctic inflow continues downstream to the Scotian Shelf and MAB. The along-shelf velocity structure resembles the mean state well (Figures 12g and 12j vs. Figures 15d and 15e), suggesting that larger-scale sub-Arctic inflow is important in setting up the mean flow downstream. The equatorward shelf flow there primarily stems from the enhanced density gradient in the cross-shelf direction. One could postulate that the inflow acting upon the buoyancy source from the St. Lawrence River carries the fresher water downstream to the Scotian Shelf and northern MAB, enhancing the thermal wind shear and thus the along-shelf flow there. Conversely, without the sub-Arctic inflow, the along-shelf transport at Scotian Shelf and northern MAB would reverse direction, going poleward (Figure 16b). Such a reversal in transport is associated with the changes of the Gulf Stream path in response to the absence of the sub-Arctic inflow (see below). As a result, the overall contribution from the sub-Arctic inflow to the along-shelf transport at the southern shelves is about 1.2–1.3 Sv (Figure 16b).

One thing worth noting is that the influence of subpolar sub-Arctic inflow on the along-shelf circulation is not limited to regions shallower than 200 m (Figure 15a). This is particularly true for the Labrador coast. As a result, for the along-shelf transport integrated from the coast to 500 m isobath, the influence of subpolar sub-Arctic inflow plays a much larger role, at 2–3 Sv or around 50% of the total transport in the control state. The contribution from the subpolar sub-Arctic inflow also decreases from the Labrador coast to the Scotian Shelf and Mid-

Atlantic Bight, a reasonable result considering the "leaky" system character (e.g., Loder et al., 1998; Lozier & Gawarkiewicz, 2001).

In addition to the equatorward along-shelf flow, the mean sea level is also significantly influenced by the sub-Arctic inflow (Figure 15a). Over the shelf and shelfbreak, the inflow contributes to the setup of sea level by ~0.5–~0.7 m, with a higher sea level over the Labrador Shelf and a lower sea level toward the MAB. The resultant along-isobath sea level tilt from Cape Hatteras to the Labrador Shelf is 2.1×10^{-8}, or two thirds of the sea level tilt from the modeled mean sea level tilt in the control configuration. The tilt is 1.6×10^{-8} on the Labrador Shelf, larger than the sea level tilt on the southern shelves (Figure 16a). This suggests that if the origin of the along-shelf pressure gradient is solely associated with the sub-Arctic inflow, the gradient would be stronger in the higher latitude. Another noteworthy result is the negative sea level change of ~ 1m with the presence of inflow off the shelfbreak (Figure 15a). Comparison of the mean states with versus without the inflow (*ctrl* vs. *closed*) clearly shows that the position of the Gulf Stream shifts shoreward along the shelfbreak in the *closed* experiment (Figure 15a). In other words, the sub-Arctic inflow and its continuation as the slope current (Flagg et al., 2006) in the subtropical NWA is a key factor in maintaining the realistic Gulf Stream position off the shelfbreak. The control of the Gulf Stream's separation from the Cape Hatteras and its post-separation position has been long discussed with diverse views including local topographic dynamics (e.g.,Schoonover et al., 2017), crossing of the Deep Western Boundary Current (DWBC) (e.g., Spall, 1996), subtropical processes (e.g., Hameed et al., 2018), and subpolar processes (e.g., Peña-Molino & Joyce, 2008; Rossby & Benway, 2000). Realistic representation of Gulf Stream position is also a long-standing issue in numerical modeling and is associated with model resolution, grid type, subgrid-scale viscosity, treatment of bathymetry, surface forcing, and wind-current interaction, to name a few (e.g., Bryan et al., 2007; Chassignet & Marshall, 2008; Ezer, 2016; Renault et al., 2016). The results from the numerical experiments here suggest that subpolar processes rather than subtropical processes likely have a larger control on the separation and position of the Gulf Stream.

The response of sea level tilt (Figure 16a) to sub-Arctic inflow is also manifested in the along-isobath pressure gradient term (Figure 17). With and without the inflow, the most sensitive term in the along-isobath momentum balance is the pressure gradient term. Over the Labrador Shelf, the (change of) pressure gradient term is consistent across the shelf, with a generally larger relative magnitude offshore, and is balanced primarily by bottom drag at the mid-Labrador section and a combination of bottom drag, Coriolis and nonlinear terms at the south Labrador section. The along-isobath pressure gradient term is non-uniform on the southern shelves (Figures 17g and 17h), indicative of the complex workings of the processes there. In comparison, the influence of the sub-Arctic inflow on the cross-isobath momentum balance is more straight-forward (Figures 17a–17d). The circulation over the shelf and shelfbreak is clearly reflected in the balance between cross-shelf pressure gradient force and Coriolis term, suggesting that the inflow is key in maintaining the geostrophic along-shelf flow on the entire NWA shelf.

4.3. Sea Ice and Remote Buoyancy/Wind Contribution

Even though the model simulations compare well with available observations, one potentially important process, the seasonally occurring sea ice on the northern shelves, is not included in the model. The impact of sea ice on the along-shelf flow in winter can be considered from the perspective of both buoyancy and momentum fluxes. While cryosphere-ocean interaction is an active area of ongoing research and quantitative assessment of the impact of sea ice on the along-shelf flow in the Northern NWA requires further development of high-fidelity sea ice models, qualitative assessment of the role of sea ice in the context of this work is possible.

Sea ice forms along the Labrador inner shelf and results in an increase of local salinity near shore (i.e., brine rejection) while spring melting, and thus seawater freshening, occurs at the marginal ice zone along the Labrador shelfbreak and near the northern flank of the Grand Banks (e.g., Fenty & Heimbach, 2013). Such a process reduces the buoyancy gradient in the cross-shelf direction and decreases the contribution of buoyancy to the mean along-shelf flow (thermal wind balance, Equation 6). Sea ice also modulates the momentum transfer from the atmosphere to the ocean. While fully packed sea ice, that is, 100% concentration, reduces momentum transfer, partial sea ice coverage amplifies the efficiency of stress input to the ocean compared to ice-free open water due to the larger drag coefficients at both the air-ice interface and ice-ocean interface associated with ice morphology (e.g., Martin et al., 2014; Martin et al., 2016; Schulze & Pickart, 2012). It has been shown that ocean surface stress generally increases with ice concentration, with optimal ice concentration for momentum transfer at ~ 80–90%, and sea ice only starts to inhibit momentum transfer (i.e., surface stress with sea ice less than open water surface

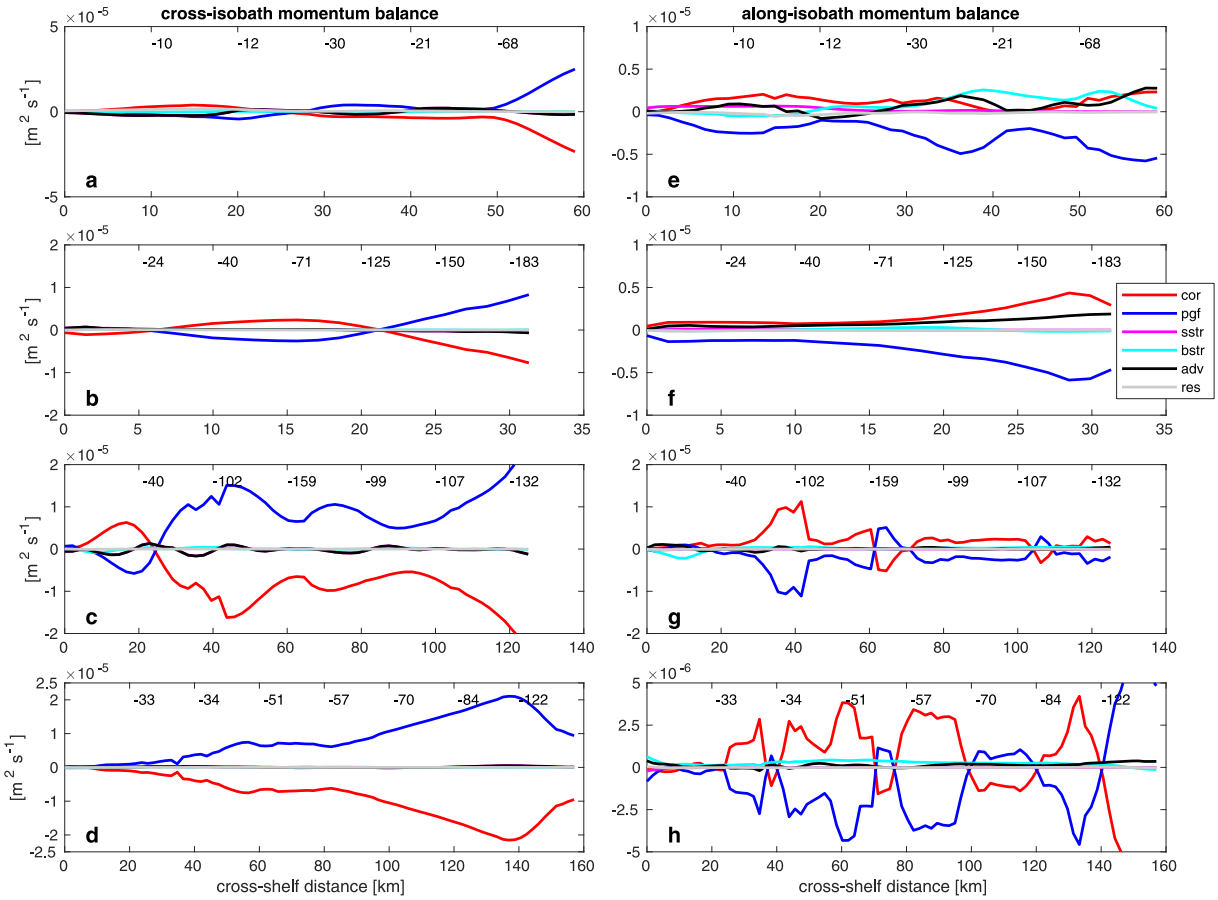

Figure 17. Differences of dynamical terms (unit $m^2\ s^{-1}$) in the cross-isobath and along-isobath momentum balance between *ctrl* and *closed* experiments at the middle Labrador section (a, e), southern Labrador section (b, f), Scotian Shelf section (c, g) and northern Mid-Atlantic Bight section (d, h). Corioils (cor), pressure gradient force (pgf), wind stress (sstr), bottom stress (bstr), nonlinear advection (adv), and residual terms (unit: $m\ s^{-2}$) are shown. *X*-axis is the cross-shelf distance from the coast with corresponding water depth (unit: meter) shown on the top of each panel. Each term is decomposed to along-isobath and cross-isobath components according to the local orientation of the isobath.

stress) at very high ice concentration approaching 100% (Martin et al., 2014, 2016). Analysis of satellite-derived ASI-AMSRE (ARTIST Sea Ice algorithm with Advanced Microwave Scanning Radiometer for EOS data) sea ice concentration data (Spreen et al., 2008) reveals that ice concentration on the Labrador shelf has large spatial and interannual variability and can reach 100% at any given days in wintertime (not shown). However, the seasonally maximum sea ice concentration averaged at the middle and southern Labrador sections (see locations in Figure 7) over the life span of AMSR-E (2002–2011) is about 92%. This number is close to the range where atmosphere-to-ocean momentum transfer is maximized (Martin et al., 2016), which suggests that for a wide range of conditions, sea ice is more likely to increase than to reduce the wind stress exerted on the ocean even in the season of maximum sea-ice coverage. In other words, including sea ice in the model would be unlikely to qualitatively change that wind stress has a larger influence on the along-shelf flow than freshwater runoff on the Labrador shelf. This hypothesis could motivate further studies of the role of seasonal sea-ice coverage in high-latitude coastal flows.

Because of the absence of a sea-ice module, the advective transport of sea ice, mainly through the northern open boundary, is also excluded in this work. Long-term observations at the Davis Strait reveal that the freshwater transport in the form of solid ice is one order of magnitude smaller than that of liquid form (Curry et al., 2014), which indicates that the northern open boundary condition in the model already incorporates the majority of the freshwater transport from higher latitudes. Further separation of the wind-driven and buoyancy-driven components in the sub-Arctic inflow is challenging and beyond the scope of this work based on regional ocean modeling. Buoyancy forcing has long been considered an important component of the circulation in the arctic-subarctic

region (e.g., Bacon et al., 2008; Sutherland & Pickart, 2008; Münchow et al., 2015, among others). On the other hand, the wind-driven two-layer model in YC21 does reproduce the East and West Greenland Currents as well as the cyclonic circulation in the Baffin Bay (Figure 4 in YC21), indicating that the sub-Arctic inflow is at least partly driven by wind stress. The complication, however, is that the current carrying the remote buoyancy source, both in solid and liquid form, can still be wind-driven (e.g., Stewart & Haine, 2013; Yang & Chen, 2021). In other words, remote buoyancy input and wind-driven circulation could be tightly coupled. A comprehensive understanding of various forms of buoyancy forcings and wind forcing on the shelf circulation could be achieved by using a well-treated, coupled circulation-sea ice model that encompasses the arctic-subarctic region.

Finally, the main subject of this work is to evaluate the importance of the local wind stress in driving the mean along-shore flow along the NWA coast when compared to the buoyancy forcing from local continental runoff, which has been largely accepted as the predominant driver. The remote influences from higher latitudes, including sea ice transport, do not directly affect this specific assessment. Nevertheless, more comprehensive studies are needed for a better understanding of how Arctic-Atlantic connections affect the NWA coastal circulations, which is beyond the scope of this study.

5. Summary and Conclusions

This study investigates the drivers of the mean shelf circulation in the NWA using a newly developed, high-resolution (2 km) regional circulation model. As one important component of this work, the local buoyancy input from glacial melt and river discharge are carefully treated and implemented. Driven by realistic oceanic, atmospheric, and continental runoff conditions, the NWA model captures the broad-scale hydrography and geostrophic flow patterns. In particular, the model compares well with in situ observations including subsurface hydrography in the GoM, coastal sea level in the Mid-Atlantic Bight, and depth-averaged velocity from Georges Bank to Cape Hatteras. These comparisons with observations in the southern (downstream) part of the NWA shelf are evidence that the northern open boundary conditions and internal configurations are properly implemented, and that the model simulates circulation dynamics to an extent appropriate for this study. Built upon the realistic configuration, idealized numerical experiments are conducted to investigate the drivers of the mean shelf circulation.

Comparative examination of the contributions of wind stress and freshwater runoff reveals their different roles of each in setting up the shelf circulation. While the freshwater runoff consistently contributes to the equatorward along-shelf flow, it has only a relatively smaller contribution to the along-shelf transport. In comparison, the wind stress has a much greater impact on the transport. Over the Labrador Shelf where the mean wind direction is approximately aligned in the along-shelf direction, wind stress is clearly more important than freshwater runoff in driving the along-shelf coastal Labrador Current and thus along-shelf transport. Without wind stress, the along-shelf transport would have been reduced significantly. On the Scotian Shelf and in the northern Mid-Atlantic Bight, the mean wind stress is against the mean along-shelf flow, that is, restricting equatorward along-shelf transport. Removing wind stress would result in an increase of along-shelf transport. Focusing on the magnitude of the influence, wind stress is consistently more important than freshwater runoff in setting up the shelf circulation system in the NWA coastal ocean. These results differ from the earlier hypothesis that emphasizes the importance of continental buoyancy input to the mean along-shelf flow (Chapman & Beardsley, 1989). The overall mean sea level on the shelf is controlled more by the wind stress as well. While both wind stress and freshwater runoff contribute similarly to the coastal sea level on the Labrador Shelf, wind stress is more dominant in determining the sea level on the southern shelves from the Mid-Atlantic Bight to the Scotian Shelf. Specifically, the current-opposing wind decreases the mean continental shelf sea level by about ∼0.1–∼0.18 m, while accumulated freshwater runoff increases the mean sea level by ∼ 0.05 m over a majority of the region, except in the Gulf of St. Lawrence where the St. Lawrence River would elevate the sea level more than 0.17 m. In other words, the wind stress is crucial in maintaining the broad-scale along-isobath sea level tilt on the NWA shelf, which has been considered important in the along-shelf momentum balance as the driving force.

Earlier 2D continental shelf models consider a balance between (barotropic) along-isobath pressure gradient force and along-isobath stress divergence for the mean circulation. This is not necessarily the case for 3D momentum balance when along-shelf variability is present (i.e., $\frac{\partial}{\partial y} \neq 0$). This is because with along-shelf variation of complex topography and transport, the mean shelf flow does not always follow the local isobath exactly, which leads to a non-zero Coriolis term in the along-shelf (along-isobath) direction along with non-negligible nonlinear terms

(Equation 8). In the cross-isobath direction, the momentum balance is largely geostrophic, which enables the use of thermal-wind balance to understand the along-shelf flow. Decomposition of the depth-averaged along-shelf current shows that the contribution of wind stress to along-shelf flow is largely a barotropic response on the Labrador Shelf and is a combination of barotropic and baroclinic response on the Scotian Shelf and in the northern Mid-Atlantic Bight. In comparison, the response of along-shelf flow to freshwater runoff is mainly baroclinic on both the Labrador shelf and the southern shelves.

In addition to the local wind stress and freshwater runoff, the role of the sub-Arctic inflow represented by the Greenland and Baffin Currents is also examined. The result highlights the importance of inflow in maintaining the equatorward shelf circulation and sea level. The sub-Arctic inflow significantly contributes to the along-shelf transport from the Labrador Shelf to Mid-Atlantic Bight. The influence of the inflow is not confined to the continental shelf: it modulates the Gulf Stream path as well. Without the sub-Arctic inflow and its continuation as the slope current, the Gulf Stream would be unrealistically close to the shelf, reversing the equatorward shelf flow. Conversely, the existence of the sub-Arctic inflow is important to keep the coastal flow on the shelf and separate the Gulf Stream from intruding the shelf circulation system.

This work provides an updated view of the mean flow on the NWA shelf by elucidating the contributions from traditionally considered local buoyancy forcing from continental runoff, wind stress and sub-Arctic inflow. The improved understanding of the mean state of this important component of current climate system allows understanding and projection of the changes under future climate scenarios.

Data Availability Statement

The numerical model simulations upon which this study is based are too large to transfer to a public repository. Instead, the model output data are archived at a local storage server. The processed model data directly used for the analyses along with visualization software are openly available at https://figshare.com/s/5dff3bc635b6e5851186 (Chen & Yang, 2024).

Acknowledgments
This work was supported by the National Science Foundation (NSF) Ocean Science Division under Grant OCE-2241407, and National Oceanic and Atmospheric Administration (NOAA) Climate Program Office (CPO) Climate Variability and Predictability (CVP) program under Grant NA20OAR4310398. KC was also supported by the Woods Hole Oceanographic Institution (WHOI) George E. Thibault Early Career Scientist Fund. Detailed and insightful feedback from Drs. Ken Brink, Steve Lentz, and Glen Gawarkiewicz on the manuscript is greatly appreciated. Numerical modeling work was conducted at WHOI High-Performance Computing cluster Poseidon with startup support to KC.

References

Bacon, S., Myers, P., Rudels, B., & Sutherland, D. (2008). Accessing the inaccessible: Buoyancy-driven coastal currents on the shelves of Greenland and eastern Canada.

Bamber, J., van den Broeke, M., Ettema, J., Lenaerts, J., & Rignot, E. (2012). Recent large increases in freshwater fluxes from Greenland into the North Atlantic. *Geophysical Research Letters*, *39*(19), L19501. https://doi.org/10.1029/2012gl052552

Beardsley, R. C., & Winant, C. D. (1979). On the mean circulation in the mid-Atlantic Bight. *Journal of Physical Oceanography*, *9*(3), 612–619. https://doi.org/10.1175/1520-0485(1979)009<0612:otmcit>2.0.co;2

Brink, K. H. (1991). Coastal-trapped waves and wind-driven currents over the continental shelf. *Annual Review of Fluid Mechanics*, *23*(1), 389–412. https://doi.org/10.1146/annurev.fluid.23.1.389

Bryan, F. O., Hecht, M. W., & Smith, R. D. (2007). Resolution convergence and sensitivity studies with North Atlantic circulation models. Part I: The western boundary current system. *Ocean Modelling*, *16*(3–4), 141–159. https://doi.org/10.1016/j.ocemod.2006.08.005

Chapman, D. C. (1985). Numerical treatment of cross-shelf open boundaries in a barotropic coastal ocean model. *Journal of Physical Oceanography*, *15*(8), 1060–1075. https://doi.org/10.1175/1520-0485(1985)015<1060:ntocso>2.0.co;2

Chapman, D. C., Barth, J. A., Beardsley, B. C., & Fairbanks, R. G. (1986). On the continuity of mean flow between Scotian Shelf and the Middle Atlantic Bight. *Journal of Physical Oceanography*, *16*(4), 758–772. https://doi.org/10.1175/1520-0485(1986)016<0758:otcomf>2.0.co;2

Chapman, D. C., & Beardsley, B. C. (1989). On the origin of shelf water in the Middle Atlantic Bight. *Journal of Physical Oceanography*, *19*(3), 384–391. https://doi.org/10.1175/1520-0485(1989)019<0384:otoosw>2.0.co;2

Chassignet, E. P., & Marshall, D. P. (2008). Gulf Stream separation in numerical ocean models. *Ocean Modeling in an Eddying Regime*, 39–61. https://doi.org/10.1029/177gm05

Chen, K., Gawarkiewicz, G., Kwon, Y.-O., & Zhang, W. G. (2015). The role of atmospheric forcing versus ocean advection during the extreme warming of the Northeast U.S. continental shelf in 2012. *Journal of Geophysical Research: Oceans*, *120*(6), 4324–4339. https://doi.org/10.1002/2014jc010547

Chen, K., Gawarkiewicz, G., & Yang, J. (2022). Mesoscale and submesoscale shelf-ocean exchanges initialize an advective marine heatwave. *Journal of Geophysical Research: Oceans*, *127*(1), e2021JC017927. https://doi.org/10.1029/2021jc017927

Chen, K., & He, R. (2010). Numerical investigation of the middle Atlantic Bight shelfbreak frontal circulation using a high-resolution ocean hindcast model. *Journal of Physical Oceanography*, *40*(5), 949–964. https://doi.org/10.1175/2009jpo4262.1

Chen, K., & He, R. (2015). Mean circulation in the coastal ocean off northeastern North America from a regional-scale ocean model. *Ocean Science*, *11*(4), 503–517. https://doi.org/10.5194/os-11-503-2015

Chen, K., Kwon, Y.-O., & Gawarkiewicz, G. (2016). Interannual variability of winter-spring temperature in the Middle Atlantic Bight: Relative contributions of atmospheric and oceanic processes. *Journal of Geophysical Research: Oceans*, *121*(6), 4209–4227. https://doi.org/10.1002/2016jc011646

Chen, K., & Yang, J. (2024). Chen and Yang 2024 Northwest Atlantic shelf mean flow paper. *Figshare*. https://doi.org/10.6084/m9.figshare.26005219

Chin, T. M., Vazquez-Cuervo, J., & Armstrong, E. M. (2017). A multi-scale high-resolution analysis of global sea surface temperature. *Remote Sensing of Environment*, *200*, 154–169. https://doi.org/10.1016/j.rse.2017.07.029

Csanady, G. T. (1976). Mean circulation in shallow seas. *J Geophys Res-Oc Atm*, *81*(30), 5389–5399. https://doi.org/10.1029/jc081i030p05389
Csanady, G. T. (1978). The arrested topographic wave. *Journal of Physical Oceanography*, *8*(1), 47–62. https://doi.org/10.1175/1520-0485(1978)008<0047:tatw>2.0.co;2
Curry, B., Lee, C. M., Petrie, B., Moritz, R. E., & Kwok, R. (2014). Multiyear volume, liquid freshwater, and Sea Ice transports through Davis Strait, 2004–10. *Journal of Physical Oceanography*, *44*(4), 1244–1266. https://doi.org/10.1175/jpo-d-13-0177.1
Dai, A. (2021). Hydroclimatic trends during 1950–2018 over global land. *Climate Dynamics*, *56*(11–12), 4027–4049. https://doi.org/10.1007/s00382-021-05684-1
Egbert, G. D., & Erofeeva, S. Y. (2002). Efficient inverse modeling of barotropic ocean tides. *Journal of Atmospheric and Oceanic Technology*, *19*(2), 183–204. https://doi.org/10.1175/1520-0426(2002)019<0183:eimobo>2.0.co;2
Emery, W. J., & Thomson, R. E. (2001). Chapter 3 - statistical methods and error handling. In W. J. E. E. Thomson (Ed.), *Data analysis methods in physical Oceanography* (pp. 193–304). Elsevier Science.
Ezer, T. (2016). Revisiting the problem of the Gulf Stream separation: On the representation of topography in ocean models with different types of vertical grids. *Ocean Modelling*, *104*, 15–27. https://doi.org/10.1016/j.ocemod.2016.05.008
Fairall, C. W., Bradley, E. F., Hare, J. E., Grachev, A. A., & Edson, J. B. (2003). Bulk parameterization of air–sea fluxes: Updates and verification for the COARE algorithm. *Journal of Climate*, *16*(4), 571–591. https://doi.org/10.1175/1520-0442(2003)016<0571:bpoasf>2.0.co;2
Fenty, I., & Heimbach, P. (2013). Coupled Sea ice–ocean-state estimation in the labrador sea and Baffin Bay. *Journal of Physical Oceanography*, *43*(5), 884–904. https://doi.org/10.1175/jpo-d-12-065.1
Flagg, C. N., Dunn, M., Wang, D., Rossby, H. T., & Benway, R. L. (2006). A study of the currents of the outer shelf and slope from a decade of shipboard ADCP observations in the Middle Atlantic Bight. *Journal of Geophysical Research*, *111*(C6), C06003. https://doi.org/10.1029/2005JC003116
Fratantoni, P. S., & Pickart, R. S. (2007). The western north Altantic shelfbreak current system in summer. *Journal of Physical Oceanography*, *37*(10), 2509–2533. https://doi.org/10.1175/jpo3123.1
Garcia, H. E., Boyer, T. P., Baranova, O. K., Locarnini, R. A., Mishonov, A. V., Grodsky, A., et al. (2019). World Ocean Atlas 2018: Product Documentation.
Haidvogel, D. B., Arango, H., Budgell, W. P., Cornuelle, B. D., Curchitser, E., Di Lorenzo, E., et al. (2008). Ocean forecasting in terrain-following coordinates: Formulation and skill assessment of the regional ocean modeling system. *Journal of Computational Physics*, *227*(7), 3595–3624. https://doi.org/10.1016/j.jcp.2007.06.016
Hameed, S., Wolfe, C. L. P., & Chi, L. (2018). Impact of the Atlantic meridional mode on Gulf Stream North Wall position. *Journal of Climate*, *31*(21), 8875–8894. https://doi.org/10.1175/jcli-d-18-0098.1
Han, G., Lu, Z., Wang, Z., Helbig, J., Chen, N., & de Young, B. (2008). Seasonal variability of the Labrador Current and shelf circulation off Newfoundland. *Journal of Geophysical Research*, *113*(C10), C10013. https://doi.org/10.1029/2007jc004376
Hannah, C. G., Shore, J. A., Loder, J. W., & Naimie, C. E. (2001). Seasonal circulation on the western and central Scotian Shelf. *Journal of Physical Oceanography*, *31*(2), 591–615. https://doi.org/10.1175/1520-0485(2001)031<0591:scotwa>2.0.co;2
Hersbach, H., Bell, B., Berrisford, P., Hirahara, S., Horányi, A., Muñoz-Sabater, J., et al. (2020). The ERA5 global reanalysis. *The Quarterly Journal of the Royal Meteorological Society*, *146*(730), 1999–2049. https://doi.org/10.1002/qj.3803
Lazier, J. R. N., & Wright, D. G. (1993). Annual velocity variations in the Labrador current. *Journal of Physical Oceanography*, *23*(4), 659–678. https://doi.org/10.1175/1520-0485(1993)023<0659:avvitl>2.0.co;2
Lellouche, J.-M., Greiner, E., Bourdallé-Badie, R., Garric, G., Melet, A., Drévillon, M., et al. (2021). The Copernicus global 1/12° oceanic and Sea Ice GLORYS12 reanalysis. *Frontiers of Earth Science*, *9*, 698876. https://doi.org/10.3389/feart.2021.698876
Lentz, S. J. (2008). Observations and a model of the mean circulation over the middle Atlantic Bight continental shelf. *Journal of Physical Oceanography*, *38*(6), 1203–1221. https://doi.org/10.1175/2007jpo3768.1
Loder, J. W., Petrie, B., & Gawarkiewicz, G. (1998). The coastal ocean off northeastern North America: A large-scale view. In A. R. Robinson & K. H. Brink (Eds.), *The Sea* (pp. 105–133).
Lozier, M. S., & Gawarkiewicz, G. (2001). Cross-frontal exchange in the middle Atlantic Bight as evidenced by surface Drifters. *Journal of Physical Oceanography*, *31*(8), 2498–2510. https://doi.org/10.1175/1520-0485(2001)031<2498:cfeitm>2.0.co;2
Martin, T., Steele, M., & Zhang, J. (2014). Seasonality and long-term trend of Arctic Ocean surface stress in a model. *Journal of Geophysical Research: Oceans*, *119*(3), 1723–1738. https://doi.org/10.1002/2013jc009425
Martin, T., Tsamados, M., Schroeder, D., & Feltham, D. L. (2016). The impact of variable sea ice roughness on changes in arctic ocean surface stress: A model study. *Journal of Geophysical Research: Oceans*, *121*(3), 1931–1952. https://doi.org/10.1002/2015jc011186
Mason, E., Molemaker, J., Shchepetkin, A. F., Colas, F., McWilliams, J. C., & Sangrà, P. (2010). Procedures for offline grid nesting in regional ocean models. *Ocean Modelling*, *35*(1–2), 1–15. https://doi.org/10.1016/j.ocemod.2010.05.007
Münchow, A., Falkner, K. K., & Melling, H. (2015). Baffin Island and West Greenland current systems in northern Baffin Bay. *Progress in Oceanography*, *132*, 305–317. https://doi.org/10.1016/j.pocean.2014.04.001
Orlanski, I. (1976). A simple boundary condition for Unbounded hyperbolic flows. *Journal of Computational Physics*, *21*(3), 251–269. https://doi.org/10.1016/0021-9991(76)90023-1
Peña-Molino, B., & Joyce, T. M. (2008). Variability in the slope water and its relation to the Gulf Stream path. *Geophysical Research Letters*, *35*(3), L03606. https://doi.org/10.1029/2007gl032183
Pringle, J. M. (2018). Remote forcing of shelf flows by density gradients and the origin of the annual mean flow on the mid-Atlantic Bight. *Journal of Geophysical Research: Oceans*, *123*(7), 4464–4482. https://doi.org/10.1029/2017jc013721
Renault, L., Molemaker, M. J., Gula, J., Masson, S., & McWilliams, J. C. (2016). Control and stabilization of the Gulf Stream by oceanic current interaction with the atmosphere. *Journal of Physical Oceanography*, *46*(11), 3439–3453. https://doi.org/10.1175/jpo-d-16-0115.1
Rossby, T., & Benway, R. L. (2000). Slow variations in mean path of the Gulf Stream east of Cape Hatteras. *Geophysical Research Letters*, *27*(1), 117–120. https://doi.org/10.1029/1999gl002356
Rypina, I. I., Chen, K., Hernández, C. M., Pratt, L. J., & Llopiz, J. K. (2019). Investigating the suitability of the Slope Sea for Atlantic Bluefin tuna spawning using a high-resolution ocean circulation model. *ICES Journal of Marine Science*, *76*(6), 1666–1677. https://doi.org/10.1093/icesjms/fsz079
Schoonover, J., Dewar, W. K., Wienders, N., & Deremble, B. (2017). Local sensitivities of the Gulf Stream separation. *Journal of Physical Oceanography*, *47*(2), 353–373. https://doi.org/10.1175/jpo-d-16-0195.1
Schulze, L. M., & Pickart, R. S. (2012). Seasonal variation of upwelling in the Alaskan Beaufort Sea: Impact of sea ice cover. *Journal of Geophysical Research*, *117*(C6), C06022. https://doi.org/10.1029/2012jc007985
Scott, J. T., & Csanady, G. T. (1976). Nearshore currents off long Island. *Journal of Geophysical Research (1896–1977)*, *81*(30), 5401–5409. https://doi.org/10.1029/jc081i030p05401

Shchepetkin, A. F., & McWilliams, J. C. (2005). The regional oceanic modeling system (ROMS): A split-explicit, free-surface, topography-following-coordinate oceanic model. *Ocean Modelling*, *9*(4), 347–404. https://doi.org/10.1016/j.ocemod.2004.08.002

Smith, P. C., & Schwing, F. B. (1991). Mean circulation and variability on the eastern Canadian continental shelf. *Continental Shelf Research*, *11*(8–10), 977–1012. https://doi.org/10.1016/0278-4343(91)90088-n

Spall, M. A. (1996). Dynamics of the Gulf Stream/deep western boundary current crossover. Part I: Entrainment and recirculation. *Journal of Physical Oceanography*, *26*(10), 2152–2168. https://doi.org/10.1175/1520-0485(1996)026<2152:dotgsw>2.0.co;2

Spreen, G., Kaleschke, L., & Heygster, G. (2008). Sea ice remote sensing using AMSR-E 89-GHz channels. *Journal of Geophysical Research*, *113*(C2), C02S03. https://doi.org/10.1029/2005jc003384

Stewart, K. D., & Haine, T. W. N. (2013). Wind-driven Arctic freshwater anomalies. *Geophysical Research Letters*, *40*(23), 6196–6201. https://doi.org/10.1002/2013gl058247

Stommel, H., & Leetmaa, A. (1972). Circulation on the continental shelf. *Proceedings of the National Academy of Sciences*, *69*(11), 3380–3384. https://doi.org/10.1073/pnas.69.11.3380

Sutherland, D., & Pickart, R. (2008). The East Greenland coastal current: Structure, variability, and forcing. *Progress in Oceanography*, *78*(1), 58–77. https://doi.org/10.1016/j.pocean.2007.09.006

Tang, C. C. L., Ross, C. K., Yao, T., Petrie, B., DeTracey, B. M., & Dunlap, E. (2004). The circulation, water masses and sea-ice of Baffin Bay. *Progress in Oceanography*, *63*(4), 183–228. https://doi.org/10.1016/j.pocean.2004.09.005

Thompson, K. R., Lazier, J. R. N., & Taylor, B. (1986). Wind-forced changes in labrador current transport. *Journal of Geophysical Research*, *91*(C12), 14261–14268. https://doi.org/10.1029/jc091ic12p14261

Townsend, D. W., Thomas, A. C., Mayer, L. M., Thomas, M. A., & Quinlan, J. A. (2006). Oceanography of the Northwest Atlantic continental shelf. In A. R. R. A. K. H. Brink (Ed.), *The Sea*. Harvard University Press.

Wang, D.-P. (1982). Effects of continental slope on the mean shelf circulation. *Journal of Physical Oceanography*, *12*, 1524–1526. https://doi.org/10.1175/1520-0485(1982)012<1524:eocsot>2.0.co;2

Wang, Z., Yashayaev, I., & Greenan, B. (2015). Seasonality of the inshore Labrador current over the Newfoundland shelf. *Continental Shelf Research*, *100*, 1–10. https://doi.org/10.1016/j.csr.2015.03.010

Warner, J. C., Sherwood, C. R., Arango, H. G., & Signell, R. P. (2005). Performance of four turbulence closure models implemented using a generic length scale method. *Ocean Modelling*, *8*(1–2), 81–113. https://doi.org/10.1016/j.ocemod.2003.12.003

Wise, A., Hughes, C. W., & Polton, J. A. (2018). Bathymetric influence on the coastal sea level response to ocean gyres at western boundaries. *Journal of Physical Oceanography*, *48*(12), 2949–2964. https://doi.org/10.1175/jpo-d-18-0007.1

Wise, A., Polton, J. A., Hughes, C. W., & Huthnance, J. M. (2020). Idealised modelling of offshore-forced sea level hot spots and boundary waves along the North American East Coast. *Ocean Modelling*, *155*, 101706. https://doi.org/10.1016/j.ocemod.2020.101706

Wu, Y., Tang, C., & Hannah, C. (2012). The circulation of eastern Canadian seas. *Progress in Oceanography*, *106*, 28–48. https://doi.org/10.1016/j.pocean.2012.06.005

Yang, J., & Chen, K. (2021). The role of wind stress in driving the along-shelf flow in the Northwest Atlantic ocean. *Journal of Geophysical Research: Oceans*, *126*(4), e2020JC016757. https://doi.org/10.1029/2020jc016757